SLAC – PUB – 3447
September 1984
T/E

EXOTIC PROCESSES IN HIGH-ENERGY *e-p* COLLISIONS*

JONATHAN A. BAGGER AND MICHAEL E. PESKIN

Stanford Linear Accelerator Center

Stanford University, Stanford, California, 94305

ABSTRACT

We survey the variety of reactions probing physics beyond the standard model which might be observed at an *e-p* collider with center-of-mass energy of order 1 TeV. We display cross-sections for numerous such reactions and assess the reach in mass or distance scale of such a collider.

Submitted to *Physical Review D*

* Work supported by the Department of Energy, contract DE – AC03 – 76SF00515

1. Introduction

The successes of the standard gauge theory of the strong, weak and electromagnetic interactions have tempted high-energy physicists to look beyond this model and to ask what physics will correct or supercede it as we push to still smaller distances. This question has prompted plans for new accelerators capable of probing such new physics, up to energy scales of order 1 TeV. The most ambitious of these proposals has been for the construction of the Superconducting SuperCollider (SSC), which would provide colliding proton beams of energy 20 TeV[1] . The physics opportunities of such a high-energy p-p collider have been reviewed in impressive detail in a recent paper by Eichten, Hinchliffe, Lane and Quigg[2] . At the same time that one investigates the physics of proton-proton collisions, however, it is worth examining other elementary particle reactions, to see if there are other methods for accessing the next stage of fundamental physics.

In this paper, we focus on the question of exploring the TeV energy scale through electron-proton collisions. Such collisions might be produced, for example, at the intersection of a relatively low-energy electron ring with a high-energy proton synchrotron. In such a scenario, the center-of-mass energy of the e-p collisions would be lower than the energy available in p-p collisions. It is not unreasonable, however, that this lowering of the available energy might be compensated by the relative cleanliness of the final states produced in e-p collisions, by the relative ease of producing novel leptonic states, and by the fact that the electron, unlike the proton, is an elementary object at the level of the standard model.

The question which we address in this paper is that of precisely how far e-p colliders of various center-of-mass energies reach into the energy regions where

new physics can be found. Our method of attacking this issue is systematic but prosaic. We begin by enumerating the various reactions that might produce exotic particles or other effects which would signal the breakdown of the standard model. We then compute the cross-sections for these processes, and establish a general picture of what new physics might be accessible with an *e-p* collider of fixed center-of-mass energy. None of the processes considered here are actually new, although some have been discussed previously only at the 1982 Snowmass summer study[3] . Our contribution in this paper will be to indicate the full breadth of new physics available at a high-energy *e-p* collider, and to provide realistic estimates of the rates which would be available at an *e-p* facility constructed at the SSC. After completing this work, we learned of an analogous and, in many ways, complementary, survey of *e-p* physics by Altarelli, Mele, and Rückl[4] .

This paper is organized as follows: Section 2 is devoted to a discussion of a number of preliminaries, including the somewhat unusual kinematics of *e-p* scattering and the rates of the dominant conventional physics processes. The remainder of the paper treats various exotic reactions, classified by parton subchannel. Section 3 discusses direct electron-quark reactions: reactions mediated by right-handed currents, processes producing supersymmetric partners of the electron and quark via gaugino exchange, and fusion of the electron and quark into a leptoquark boson. Section 4 examines processes which occur in photon-quark or photon-electron reactions: excited quark and electron production as well as production of supersymmetric partners via off-shell quark or electron intermediate states. We also discuss the possibility of lepton-gluon fusion into a color octet leptonic state. Section 5 treats new particle production via photon-gluon

fusion. Section 6 discusses the effects of the contact interactions which might result from composite quarks and leptons[5] ; our discussion follows the work of Rückl[6] . Section 7 presents some general conclusions.

2. Some Preliminaries

Before we can begin to discuss the magnitudes of various exotic reactions at a high-energy *e-p* collider, we should first clarify the energy region we will examine and the rates of conventional physics processes in this region. We will also need to discuss the special kinematics of *e-p* scattering.

The schemes envisioned for achieving very high center-of-mass energies in *e-p* collisions involve the interaction of an electron beam in a conventional electron synchrotron with a proton beam of much higher energy. The HERA proposal calls for 30 GeV electrons colliding with 800 GeV protons. The various options which have been proposed for the SSC are even more asymmetrical, since they make use of the 20 TeV circulating proton beam available there[7] . This asymmetry implies that, even though a typical quark carries only a fraction of the total momentum of the proton, the kinematics of electron-quark reactions is skewed severely toward the quark direction. Figure 1 shows the result of this asymmetry; it indicates the shape of the ellipses in momentum space locating the final states of electron-quark elastic scattering, for quarks with momentum fractions $x = 0.5$ and $x = 1$.

The forward nature of the kinematics makes it difficult to identify specific final states, since such detection would be possible only if the produced particles are sufficiently well separated from the beam direction. In our computations, we have modelled this effect in a relatively crude way by restricting the products of

the elementary parton reactions to be separated from the beam direction by more than a fixed lab-frame angle. The calculations reported here set this minimum angle at 2° and 10°.

The bulk of the cross-section for any high-energy *e-p* facility will be made up of processes already present in the standard model. Figure 2 shows the three most important of these standard processes: neutral- and charged-current deep inelastic scattering and quark pair production via the photon-gluon fusion process. The expected luminosity for an *e-p* collider associated with the SSC is of the order of 10^{32} cm^{-2} sec^{-1}; this corresponds to 1,000 events per year resulting from a cross-section of 1 picobarn. We should therefore make clear what cuts on Q^2 or transverse momentum are necessary to reduce these background processes to the picobarn level.

For unpolarized *e-p* scattering, the neutral current cross-section is given by:

$$\frac{d^2\sigma}{dxdy} = \frac{\pi\alpha^2}{sx^2y^2} \cdot \sum_f \Big\{ xf_f(x)\Big(A_f(Q^2) + (1-y)^2 B_f(Q^2)\Big) + xf_{\bar{f}}(x)\Big(B_f(Q^2) + (1-y)^2 A_f(Q^2)\Big)\Big\}, \tag{2.1}$$

where the sum runs over quark flavors, $f_f(x)$ and $f_{\bar{f}}(x)$ are the quark and anti-quark distribution functions, respectively, and $Q^2 = xys$. The functions A_f and B_f are given by

$$\begin{aligned} A_f(Q^2) &= \Big(-\mathcal{Q}_f + g_{Lf}g_{Le}\frac{Q^2}{Q^2+m_Z^2}\Big)^2 + \Big(-\mathcal{Q}_f + g_{Rf}g_{Re}\frac{Q^2}{Q^2+m_Z^2}\Big)^2 \\ B_f(Q^2) &= \Big(-\mathcal{Q}_f + g_{Rf}g_{Le}\frac{Q^2}{Q^2+m_Z^2}\Big)^2 + \Big(-\mathcal{Q}_f + g_{Lf}g_{Re}\frac{Q^2}{Q^2+m_Z^2}\Big)^2. \end{aligned} \tag{2.2}$$

Here $\mathcal{Q}_f$ denotes the quark electric charge, and g_{Li} and g_{Ri} are the left- and

right-handed Z^0 charges:

$$g_{Li} = (I_L^3 - \mathcal{Q}_i \sin^2\theta_w)/\sin\theta_w\cos\theta_w \ ; \ g_{Ri} = -\mathcal{Q}_i \sin^2\theta_w/\sin\theta_w\cos\theta_w \ .$$

Figure 3 shows the value of the cross-section which follows from (2.1), integrated over a kinematic region whose boundary is given by the angular constraints described previously and by a minimum value of Q^2. In this evaluation, and throughout this paper where the values of structure functions are required, we have used those given by EHLQ[2] . The structure functions recently presented by Duke and Owens[8] give very similar results, both here and elsewhere. We see that neutral-current cross-sections of order 1 picobarn are reached at relatively modest values of Q^2. Note that the angular cuts have a stronger effect at large values of Q^2, since these correspond to larger values of x and therefore to more extremely skewed kinematics.

The charged-current cross-section (again, for unpolarized e-p scattering) can be computed in a very similar way. The cross-section is given by

$$\frac{d^2\sigma}{dxdy} = \frac{\pi\alpha^2}{4\sin^4\theta_w s x^2 y^2} \times \left\{ \sum_u x f_u(x) \left(\frac{Q^2}{Q^2+m_W^2} \right)^2 + \sum_d x f_{\bar{d}}(x)(1-y)^2 \left(\frac{Q^2}{Q^2+m_W^2} \right)^2 \right\} , \tag{2.3}$$

where u and d run over all up- and down-type quarks. The numerical value of the charged-current cross-section, for various cuts on Q^2 and angle, is shown in Fig. 4.

The final standard process, photon-gluon fusion, is actually the dominant process at high energy, taking over the e-p cross-section in much the same way

as the 2-photon process takes over the e^+-e^- total cross-section as the energy increases. The elementary cross-section for the production of a given quark pair is

$$\frac{d\hat{\sigma}}{d\hat{t}}(\gamma + g \to q + \bar{q}) = \frac{\pi \mathcal{Q}_f^2 C(r) \alpha \alpha_s}{\hat{s}^2} \cdot \left(\frac{\hat{t} - m^2}{\hat{u} - m^2} + \frac{\hat{u} - m^2}{\hat{t} - m^2} + \frac{4m^2 \hat{s}}{(\hat{t} - m^2)(\hat{u} - m^2)} - \frac{4m^4 \hat{s}^2}{(\hat{t} - m^2)^2 (\hat{u} - m^2)^2} \right), \tag{2.4}$$

where m is the mass of the quark, $\mathcal{Q}_f$ is its electric charge, and $C(r)$ is the color factor, equal to 1 for quarks and given by

$$C(r) = \frac{1}{4} d_r C_2(r) \tag{2.5}$$

for particles in an arbitrary color representation r, of dimension d_r. The total cross-section for quark pair production, assuming six flavors and ignoring the top quark mass, is shown in Fig. 5. This process is very substantial, even with a stringent cut on the transverse momentum of the produced jets. Fortunately, the bulk of the events produced in photon-gluon fusion contain only two narrow, simple jets; they are easily distinguished from the decay products of heavy, exotic particles.

3. Electron-Quark Processes

Having now clarified the general setting of our study and displayed the rates at which the dominant processes occur, we now begin enumerating the possibilities for more exotic reactions. We will proceed channel by channel. The electron-quark channel is a natural place to begin: Since the electron has the full energy of its beam and a quark might carry a substantial fraction of the energy of the proton, higher parton center-of-mass energies are available in this reaction than in any other. On the other hand, one is constrained to consider only these reactions which involve the specified quantum numbers available, and only those novel particles which couple directly to the familiar fermions. Two such reactions are the production of new quarks and leptons by the exchange of new, heavier W bosons, perhaps with right-handed couplings, and the production of the supersymmetric partners of the e and q by exchange of the fermionic partners of the photon and Z^0. One might also consider an s-channel leptoquark resonance which couples directly to e-q. Let us discuss each of these various possibilities in turn.

The cross-section for reactions mediated by new W boson exchange is readily obtained from the considerations of the previous section: For unpolarized e-p scattering, and ignoring the masses of the produced fermions, the cross-section is the same as that given in eq. (2.3) , with m_W replaced by the mass of the new boson and $g_w = e/\sin^2\theta_w$ replaced by the new coupling constant. Figure 6 shows an estimate of the total rate for reactions involving heavy W exchange, estimated using g_w as the coupling constant (assuming, for example, an underlying left-right symmetry.). In the case in which the new exchange is mediated by a right-handed current, one could readily enhance this over the background

of standard W exchanges by polarizing the electron beam. We should note that rather stringent constraints already exist on the possible masses and couplings of right-handed W's. A Berkeley-TRIUMF experiment[9] restricts the mass of any right-handed W that mediates μ decay to be greater than 380 GeV. Analyses of the K_L-K_S system rule out any right-handed exchanges among conventional quarks mediated by bosons with mass less than several TeV[10,12] . These constraints do not eliminate the possibility that right-handed W's might mediate the production of new quarks and leptons. It is entirely possible that these new particles might lie within the energy range accessible to a high-energy e-p facility.

Supersymmetric partners of the electron and quark may be produced through direct electron-quark interactions of the type shown in Fig. 7, a process studied for lower-energy applications by Hinchliffe and Leveille[13] , Jones and Llewellyn Smith[14] , and Salati and Wallet[15] . The values of the various diagrams shown in this figure are strongly affected by the relative masses assumed for the bosonic and fermionic superpartners and by the pattern of mixing assumed between the gauge fermions and the superpartners of the Higgs bosons. We have chosen to estimate the cross-section by choosing the simplest possible form for this mixing: We assume that the $\widetilde{Z}$ mixes with only one linear combination of the Higgs superpartners, and that this linear combination has the following Majorana mass matrix:

$$\begin{pmatrix} 0 & m_Z \\ m_Z & 0 \end{pmatrix} \tag{3.1}$$

We also assume a similar mixing for the $\widetilde{W}$. The $\widetilde{Z}$ and $\widetilde{W}$ then acquire masses equal to m_Z and m_W, respectively. We consider the mass of the photino to be, to a good approximation, zero. This pattern of mixing is can actually be realized,

with a choice of parameters, in some phenomenological models of supergravity[16]; it is, in any event, a representative case among more complex mixing patterns.[17] We should note that in this particular scheme of mixing, left-handed electrons interact only with right-handed quarks and with the antiquarks of left-handed quarks.

Under these assumptions, the elementary cross-section for $e + q \to \tilde{e} + \tilde{q}$ is given by:

$$\frac{d\hat{\sigma}}{d\hat{t}} = \frac{\pi\alpha^2}{\hat{s}^2} \cdot E_{eq}(\hat{t}) \cdot (-\hat{s}\,\hat{t} - (m_e^2 - \hat{t})(m_q^2 - \hat{t})), \tag{3.2}$$

where m_e and m_q are, respectively, the masses of the $\tilde{e}$ and $\tilde{q}$, and E_{eq} is given by:

$$E_{eq}(\hat{t}) = \left\{ \frac{-\mathcal{Q}_f}{\hat{t}} + \frac{g_{Le}g_{Rf}}{\hat{t} - m_Z^2} \right\}^2 + \left\{ \frac{-\mathcal{Q}_f}{\hat{t}} + \frac{g_{Re}g_{Lf}}{\hat{t} - m_Z^2} \right\}^2 \tag{3.3}$$

The cross-section for the corresponding reaction involving $e + \bar{q}$ is obtained by interchanging g_{Lf} and g_{Rf} in the definition of $E(\hat{t})$. These two processes are of course experimentally indistinguishable. Both, though, should be quite characteristic, since the decay of the two superpartners into ordinary fermions plus two uncorrelated photinos should create a transverse momentum imbalance of the same order as the transverse momentum actually visible in the event. Figs. 8 and 9 display the cross-section for this process for two extreme cases of the ratio of $\tilde{e}$ and $\tilde{q}$ masses: first, setting $m_e = m_q$ and, secondly, setting $m_e \ll m_q$.

The rate for the process of superpartner production by $\widetilde{W}$ exchange can be estimated in the same way as the neutral-current process we have just considered. In our simple pattern of $\widetilde{W} - \widetilde{H}$ mixing, this process proceeds only in the electron-antiquark reaction. The elementary cross-section is given again by eq. (3.2), with

the function

$$E_{\nu\bar{d}}(\hat{t}) = \left\{ \frac{1}{2\sin^2\theta_w\,(\hat{t} - m_Z^2)} \right\}^2 \tag{3.4}$$

considered to be nonzero for down-type antiquarks only. The corresponding e-p cross-section in shown in Fig. 10.

In addition to t-channel exchanges, one should also consider the possibility of s-channel resonances in e-q reactions. If such a resonance could be reconstructed, it would show up in a very striking way: The constraint that the resonance have fixed mass requires that the electron pick out a quark or antiquark with a fixed value of x. This implies that resonance is produced with a characteristic energy and momentum relative to the lab frame:

$$\gamma = \frac{E_R}{M_R} = \frac{M_R^2 + 4E_e^2}{4E_e M_R}, \tag{3.5}$$

where E_e is the energy of the electron beam and M_R is the mass of the resonance. The resonance will be reconstructible provided that its boost γ is not too large: eq. (3.5) gives as a rough criterion $M_R \gtrsim 40\ E_e$. The cross-section for production of such a resonance R is given by

$$\hat{\sigma}(e + \bar{q} \to R) = \frac{4\pi^2}{M_R}(2J_R + 1)\Gamma_{R\to e\bar{q}}\delta(\hat{s} - M_R^2), \tag{3.6}$$

where $\Gamma_{R\to e\bar{q}}$ is the partial width for the decay of R to $e\bar{q}$.

Technicolor theories which contain a full generation of technifermions[18] predict the existence of a set of spinless bosons with lepton + antiquark (and possibly also lepton + quark) quantum numbers. These particles are technifermion-antitechnifermion bound states (technipions); they decay via the interactions

which connect technifermions with ordinary fermions. Since these are also the interactions responsible for generating the masses of the ordinary fermions, technipion decays are expected to favor the heaviest fermions available. The optimal process for technipion production in *e-p* reactions should be the fusion of an electron with a top antiquark in the proton. The leptoquark cross-section can be computed from the estimate of the partial width:

$$\Gamma_{R\to e\bar{t}} = \frac{G_F M_R^3}{4\pi\sqrt{2}} \cdot \left(\frac{m_t}{M_R} \cdot \sin\beta\right)^2, \tag{3.7}$$

where G_F is the Fermi constant and β is a mixing angle reflecting the limited tendency for such a boson to decay to an electron rather than, say, a τ lepton. β should properly be considered an unknown parameter, although it is unlikely to be large. Setting $\sin\beta = 0.1$ and $m_t = 40$ GeV, and integrating over the top quark distribution given by EHLQ, we find the cross-section displayed in Fig. 11. For the canonical value[19] of 160 GeV for the leptoquark mass, the cross-section seems large enough to be observable even with a relatively low-energy electron beam; this conclusion, however, depends strongly on the actual value of β.

4. Photon-Quark and Photon-Electron Processes

Exotic final states with the quantum numbers of a single lepton or quark can be reached by the interaction of electrons or quarks with photons radiated by the opposite beam. This process is not as efficient for producing high-mass states as the *e-q* subprocess, but it has the advantage that it can access, in principle, any possible higher-mass state of a quark or electron. Two typical processes, which may occur either on the quark side or on the lepton side, are the promotion

of a fermion f to an excited state f^*, which might be expected if the fermion is composite, and the associated production of supersymmetric partners of the fermion and a gauge boson. One might also imagine the production of a resonance in electron-gluon processes. We will consider each of these various possibilities in turn.

Gauge-invariance prohibits a direct vector coupling of a light fermion f to an excited state f^*. A suitable form for this coupling is of the magnetic moment form, as indicated in Fig. 12. The interaction term has a dimensionful coefficient, which we parametrize in the following way: Since the magnetic moment operator flips helicity, its coefficient should be proportional to the strength of chiral symmetry violation in the theory; a relatively conservative measure of this symmetry-breaking is the value of the f^* mass, m_*. The remaining dimensions are assigned to a parameter Λ, which, in composite models, is roughly the inverse size of the composite structure[20] . It is not at all certain what value one should assign for Λ. One should note that an analogous composite-state size parameter is constrained by Bhabha scattering to have a value greater than about 1.2 TeV[21]

The magnetic moment coupling shown in Fig. 12 leads to an elementary production cross-section

$$\widehat{\sigma}(\gamma + f \to f^*) = 4\pi^2 \mathcal{Q}_f^2 \alpha \left(\frac{m_*}{\Lambda}\right)^4 \delta(\widehat{s} - m_*^2). \tag{4.1}$$

For q^* production, this may be converted to a physical cross-section by integrating with the Weizsacker-Williams distribution of photons in the electron

$$x f_\gamma(x) = \frac{\alpha}{2\pi}(1 + (1-x)^2) \log(\widetilde{s}/4m_e^2) \tag{4.2}$$

(where $\tilde{s}$ is the square of the electron-quark subenergy) and with the relevant quark distribution function. For e^* production, the analogue of (4.2) for the proton should be used. The results, computed using the value 2 TeV for Λ, are shown in Figs. 13 and 14. Events in which such excited fermions are produced should have a very characteristic signature—a single photon recoiling against an electron or a hadron jet with fixed combined invariant mass—but the figures indicate that the cross-sections for these processes are very low for reasonable values of Λ.

In addition to directly producing new particles which are excited states of light fermions, γ-q and γ-e collisions can produce off-shell states of the original light fermions, which can then decay into new particles. This reaction provides a second mechanism for producing supersymmetric particles in e-p reactions,[13,15] leading to the processes $ep \to \tilde{q}\tilde{g}$ and $ep \to \tilde{e}\tilde{\gamma}$ (where $\tilde{g}$ and $\tilde{\gamma}$ are the gluino and photino, respectively) through the Feynman diagrams of Fig. 15. Both processes may be observed as reactions with an apparent unbalanced transverse momentum; although the effect should be neither as large nor as characteristic as for the process producing both $\tilde{q}$ and $\tilde{e}$. The diagrams of Fig. 15(a) lead to the elementary cross-section for the production of a gluino and the superpartner of a quark of given helicity, in the limit in which the $\tilde{g}$ is very light compared to the $\tilde{q}$[‡1]

$$\frac{d\hat{\sigma}}{d\hat{t}}(\gamma + q_f \to \tilde{q}_f + \tilde{g}) = \frac{4\pi\alpha\alpha_s \mathcal{Q}_f^2}{3\hat{s}^2}\left\{-\frac{\hat{u}}{\hat{s}} - \frac{(\hat{s}-2M^2)\hat{t}}{\hat{s}(\hat{t}-M^2)} + \frac{\hat{t}(\hat{t}+M^2)}{(\hat{t}-M^2)^2}\right\}, \quad (4.3)$$

where M is the mass of the $\tilde{q}$. We can obtain an idea of the numerical importance of this cross-section by considering all quark partners to have the same mass (so

‡1 This formula agrees with that of ref. 13 up to some minor misprints there.

that we can sum over helicities by multiplying (4.3) by 2), and then integrating this cross-section over the quark and photon distribution functions. The The notation is as in Fig. 6. result is shown in Fig. 16. The cross-section for $e+\gamma \to \tilde{e}+\tilde{\gamma}$ can be obtained from the formula (4.3) by simply replacing the factor $(\frac{4}{3}\alpha_s \mathcal{Q}_f^2)$ by (α). Integrating over the Weiszacker-Williams photon spectrum of the proton yields the result shown in Fig. 17. Both of these cross-sections are relatively small compared to the cross-section for $\tilde{e}$-$\tilde{q}$ production considered in the previous section.

In addition to photon-fermion reactions, we might also consider the possibility that a gluon contained in the proton will excite the electron to some novel state[22] . It is not at all unlikely that, if electrons and quarks are composite structures, their constituents carry color. Then the ground state configurations should carry the minimal color and belong to singlet or triplet representations. Higher excited states, however, could have a different internal color configuration. This would allow the same constituents to sum to a color **8** or **10**, for leptons, or a color **6** or **15**, for quarks. If the electron has a color octet excited state $\mathcal{L}_8$, this state might be produced through a magnetic moment interaction such as that shown in Fig. 12 but involving an external gluon rather than an external photon. The elementary cross-section for $\mathcal{L}_8$ production which follows from this hypothesis is a simple variation on eq. (4.1):

$$\hat{\sigma}(g + e \to \mathcal{L}_8) = 4\pi^2 \alpha_s \left(\frac{m_*}{\Lambda}\right)^4 \delta(\hat{s} - m_*^2), \tag{4.4}$$

where m_* is now the mass of the $\mathcal{L}_8$. The physical cross-section following from (4.4), shown in Fig. 18, is quite substantial. The production of the $\mathcal{L}_8$ should be

clearly visible as a class of events containing an electron-jet system with definite mass and definite energy (3.5) with respect to the lab.

5. Photon-Gluon Processes

Continuing in the direction of reactions successively less constrained by quantum numbers, we now discuss the production of exotic particles in photon-gluon fusion. This reaction can, in principle, produce any particle which has both strong and electromagnetic interactions, irrespective of its other quantum numbers. One pays a price, of course, in that normally a γ-g reaction involves only a small fraction of the total e-p center-of-mass energy.

We should first survey the results of the simple photon-gluon fusion process,[23] the production of some new species of fermion or boson *via* the diagrams of Fig. 19. For the production of new fermions, the elementary cross-section is given precisely by eq. (2.4), setting m equal to the mass of the new species. The analogous elementary cross-section for the production of a boson pair is:

$$\frac{d\hat{\sigma}}{d\hat{t}}(\gamma + g \to b + \bar{b}) = \frac{\pi \mathcal{Q}_b^2 C(r) \alpha \alpha_s}{\hat{s}^2} \times \left(1 - \frac{2m^2\hat{s}}{(\hat{t} - m^2)(\hat{u} - m^2)} + \frac{2m^4\hat{s}^2}{(\hat{t} - m^2)^2 (\hat{u} - m^2)^2} \right) . \tag{5.1}$$

To estimate the size of the physical cross-sections which follow from these results, we have evaluated the convolution of these cross-sections with the photon and gluon distribution functions. We have considered the pair-production of a new heavy quark with charge $+\frac{2}{3}$, as well as the pair production of the supersymmetric partner of such a heavy quark (counting one charged boson for each helicity, and

assigning each of these bosons the same mass m). The results are shown in Figs. 20 and 21.

In technicolor theories which predict a rich complement of Goldstone bosons, many of these bosons carry both color and electric charge[18] and can be produced by the photon-gluon fusion mechanism. In Fig. 22, we show the cross-section for the production of technipions for a technicolor model with one generation of technifermions, assumed to belong to a complex representation of the technicolor group. These bosons have been assigned the masses computed in ref. 19. At very high center-of-mass energies for the elementary process, the production of technipion pairs should be enhanced by coupling to resonances of the strong technicolor dynamics[24] . However, this effect is not important for the range of *e-p* center-of-mass energies we consider here. There are two reasons for this. First, only reactions in which the parton center-of-mass energy is below 750 GeV contribute significantly to the physical cross-sections shown in Figs. 20–22. Secondly, because the group matrices with which the photon and the gluon couple to fermions commute with one another, the technipions are produced only in even partial waves so the prominent techni-rho resonance does not contribute to *ep* reactions.

In addition to pair-production processes, the photon-gluon channel might also include single production of color octet boson resonances. Techicolor models, again, contain technipions with the correct quantum numbers to appear in this reaction. The general formula for the rate of resonance production in γ-g processes is:

$$\hat{\sigma}(\gamma + g \to R) = \frac{4\pi^2}{M_R}(2J_R + 1)\Gamma_{R\to\gamma g}\delta(\hat{s} - M_R^2), \qquad (5.2)$$

where $\Gamma_{R\to\gamma g}$ is the partial width for the decay of R to γg. In the model of ref. 18, the width of the appropriate technipion into a photon and a gluon is given by[25,24]

$$\Gamma_{R\to\gamma g} = \frac{G_F M_R^3}{4\pi\sqrt{2}} \cdot \frac{N_{TC}^2}{4} \cdot \frac{\alpha\alpha_s}{\pi^2}. \qquad (5.3)$$

The corresponding physical cross-section is displayed in Fig. 23. Just as we saw in the case of the single production of the leptonquark boson, the cross-section for producing this technipion, at the canonical value of its mass[19] , is small, but not unreasonably so.

At the same time that one discusses photon-gluon processes, one should also devote at least a little attention to photon-photon processes. In general, these cross-sections are quite small, roughly two orders of magnitude below the already marginal rates for γ-g reactions. One such reaction, however, is of sufficient importance that it is worth considering in any event: The most efficient way to produce the Higgs boson of the standard model in e-p collisions is as a resonance in photon-photon reactions. The cross-section may be obtained in terms of the 2-γ width of the Higgs and its mass M_H *via* the formula:

$$\hat{\sigma}(\gamma+\gamma\to H) = \frac{8\pi^2}{M_H}(2J_H+1)\Gamma_{H\to\gamma\gamma}\delta(\hat{s}-M_H^2). \qquad (5.4)$$

Electron-proton reactions of the energies we consider might access the Higgs if its mass is in the range of one to several hundred GeV; in this region the 2-γ width of the Higgs is dominated by the W-boson loop contribution. This contribution was computed by Ellis, Gaillard, and Nanopoulos[26] , for the case $M_H \ll m_W$, and later, in full detail, by Leveille[27] . Adding also the top quark contribution[28]

, one finds:

$$\Gamma(H \to \gamma + \gamma) = \frac{\alpha^2}{8\sqrt{2}\pi^3} G_F M_H^3 |I|^2, \tag{5.5}$$

where $I = I_W + I_t$,

$$\begin{aligned} I_W &= -\left(\frac{1}{2} + 3\frac{m_W^2}{M_H^2}\right) - \left(\frac{3}{2} - 3\frac{m_W^2}{M_H^2}\right) \mathbf{F}(M_H^2/m_W^2), \\ I_t &= \frac{3}{2} Q_t^2 \Big(4\frac{m_t^2}{M_H^2} + (1 - 4\frac{m_t^2}{M_H^2}) \mathbf{F}(M_H^2/m_t^2)\Big), \end{aligned} \tag{5.6}$$

and

$$\mathbf{F}(x) = \begin{cases} \frac{4}{x}\Big(\sin^{-1}(\frac{\sqrt{x}}{2})\Big)^2 & x < 4 \\ \frac{1}{x}\Big(\pi^2 - \frac{1}{4}\log^2(\frac{\sqrt{x}}{2} - (\frac{x}{4} - 1)^{\frac{1}{2}}) - i\pi \log(\frac{\sqrt{x}}{2} - (\frac{x}{4} - 1)^{\frac{1}{2}})\Big) & x > 4 \end{cases} \tag{5.7}$$

The corresponding physical cross-section (for $m_t = 40$ GeV) is shown in Fig. 24; it is disappointingly small.

6. Contact Interactions

Thus far, we have considered only exotic processes which involve the production of new particles. There is, however, one important process which probes physics beyond the standard model that involves only the two-body scattering of familiar light fermions. Eichten, Lane, and Peskin[5] have pointed out that, if quarks and leptons are composite, they should possess additional interactions beyond those of the standard model, which result from the exchange or interaction of their constituents in very short-range encounters. The natural range for such an interaction is the inverse of the compositeness scale Λ, defined above eq.

(4.1). If the center-of-mass energy of the fermion-fermion process is much less than this scale ($\hat{s} \ll \Lambda^2$), the new interaction may be considered to be approximately pointlike, and may be parametrized as a 4-fermion contact interaction with coupling constant set (by dimensional analysis) to be of order Λ^{-2}. Rückl[6] has studied the effects of such contact interactions with some care for the energy range of HERA. In this section, we extend Rückl's analysis to the region of TeV center-of-mass energies.

The most general *e-q* four-fermion helicity-conserving interaction which preserves both electron and quark number contains 12 distinct terms, even for a single flavor of quark. In a complete phenomenological analysis, each term should be given an independent coefficient. Our purpose here, however, is only to ascertain the magnitude of the effects of such contact interactions; for that purpose, it suffices to explore in detail a few representative examples. We choose, then, to examine the effects of contact interactions of the two forms:

$$\frac{4\pi}{\Lambda^2}\bar{e}_L\gamma^\mu e_L\bar{q}_L\gamma_\mu q_L \qquad \text{and} \qquad \frac{4\pi}{\Lambda^2}\bar{e}_L\gamma^\mu e_L\bar{q}_R\gamma_\mu q_R. \tag{6.1}$$

Let us refer to these as the LL and LR interactions, respectively. We should note that one obtains almost the same results using, in the same notation, the RR and RL contact interactions; the only difference arises from the relatively small interference term between the contact interaction and the Z^0-exchange diagram.

The interactions (6.1) lead to changes in the standard neutral current cross-section (2.1). For LL interactions, the functions $A_f(Q^2)$ and $B_f(Q^2)$ are modified

as follows:

$$A_f(Q^2) \to A_f(Q^2) + 2\,\alpha^{-1}\Big(\frac{Q^2}{\Lambda^2}\Big)\Big[Q_f - g_{Le}g_{Lf}\Big(\frac{Q^2}{Q^2+m_Z^2}\Big) + \frac{1}{2}\,\alpha^{-1}\Big(\frac{Q^2}{\Lambda^2}\Big)\Big]$$

$$B_f(Q^2) \to B_f(Q^2)\ . \tag{6.2}$$

For LR interactions, they become

$$A_f(Q^2) \to A_f(Q^2)$$

$$B_f(Q^2) \to B_f(Q^2) + 2\,\alpha^{-1}\Big(\frac{Q^2}{\Lambda^2}\Big)\Big[Q_f - g_{Le}g_{Rf}\Big(\frac{Q^2}{Q^2+m_Z^2}\Big) + \frac{1}{2}\,\alpha^{-1}\Big(\frac{Q^2}{\Lambda^2}\Big)\Big]\ . \tag{6.3}$$

Note that the changes induced by the contact interactions are of order $\alpha^{-1}(Q^2/\Lambda^2)$. They are important even at energies $Q^2 \ll \Lambda^2$.

Following Rückl, we present our results in terms of the neutral current structure function $F_2(x,Q^2)$,

$$F_2(x,Q^2) = \frac{d\sigma}{dx\,dy}\Big/\frac{2\pi\alpha^2 s}{Q^4}[1+(1-y)^2]\ . \tag{6.4}$$

The normalization is such that one recovers the usual neutral current structure $F_2(x,Q^2)$ if only one-photon exchange contributes. Some typical results for $F_2(x,Q^2)$ are shown in Figs. 25–27. The predicted deviations from the standard model, even for Λ of order 5 TeV, are quite large. In interpreting these figures, however, one must remember that the available sample of events falls rapidly with increasing Q^2. From Fig. 3, we can see that there should be only about 100 events per year in the region to the right of Q = 500 GeV, in Fig. 25; Q = 600 GeV, in Fig. 26; or Q = 800 GeV, in Fig. 27. The predicted deviations, however, are sufficiently large that experiments should certainly be sensitive to the effects of Λ at the levels indicated by these figures.

7. Conclusions

We have now completed our survey of exotic processes to be searched for and perhaps discovered in high-energy *e-p* reactions. We have attempted to systematically review all of the channels which *e-p* collisions make available, and to evaluate representative cross-sections to ascertain to what values of mass or energy each channel can probe. We have found that, in general, the elementarity of the electron does not compensate its relatively low energy in the hypothetical machines which we have considered. In most of the reactions we have discussed, only particles of mass up to roughly 200 GeV can be reached effectively. The exceptions to this rule, however, are rather interesting, if quite specific in their quantum numbers: *e-p* machines are quite effective in producing supersymmetric partners through the reaction $e + q \rightarrow \tilde{e} + \tilde{q}$ and in searching for colored excited states of leptons; they are also very sensitive to deeply suppressed contact interactions which might affect *e-q* elastic scattering. The ability of *e-p* colliders to probe these quantum-number-specific reactions might allow such colliders to provide surprising results complementary to those of high-energy *p-p* or $p\text{-}\bar{p}$ interactions.

ACKNOWLEDGEMENTS

We are grateful to Charlie Prescott and Dick Taylor for their encouragement to conduct this study, and to Stan Brodsky, Howard Haber, Helen Quinn, and Hallsie Reno, for their advice and assistance.

REFERENCES

1. S. Wojcicki, *et. al.*, Report of the 1983 Subpanel on New Facilities for the U. S. High Energy Physics Program of the High Energy Physics Advisory Panel. (U. S. Department of Energy, Wahington, 1983)
2. E. Eichten, I. Hinchliffe, K. D. Lane, and C. Quigg, Fermilab preprint FERMILAB-Pub-84/17-T / LBL-16875 / DOE/ER/01545-345 (1984)
3. Proceedings of the 1982 DPF Summer Study on Elementary Particle Physics and Future Facilities, R. Donaldson, R. Gustafson, and F. Paige, eds. (AIP, 1982)
4. G. Altarelli, B. Mele, and R. Rückl, CERN preprint CERN-TH.3932/84 (1984)
5. E. Eichten, K. D. Lane, and M. E. Peskin, Phys. Rev. Lett. 50, 811 (1983)
6. R. Rückl, Phys. Lett. 129B, 363 (1983); Nucl. Phys. B234, 91 (1984)
7. C. Y. Prescott, in Summary Report of the PSSC Discussion Group Meetings, P. Hale and B. Winstein, eds. (Fermilab, 1984)
8. D. Duke and J. F. Owens, Phys. Rev. D30, 49 (1984)
9. J. Carr. *et. al.*, Phys. Rev. Lett. 51, 627 (1983)
10. G. Beall, M. Bander, and A. Soni, Phys. Rev. Lett. 48, 848 (1982)
11. M. H. Reno and F. Gilman, Phys. Lett. 127B, 426 (1983); Phys. Rev. D29, 937 (1984)
12. I. Bigi and J. M. Frère, Phys. Lett. 129B, 469 (1984)
13. Cited by I. Hinchliffe and L. Littenberg, in ref. 3.
14. S. K. Jones and C. H. Llewellyn Smith, Nucl. Phys. B217, 145 (1983)

15. P. Salati and J. C. Walet, Phys. Lett. B122, 397 (1983)

16. R. Arnowitt, A. H. Chamseddine, and P. Nath, Phys. Rev. Lett. 50, 232 (1983)

17. For a discussion of the varieties of $\widetilde{Z}$-$\widetilde{H}$ mixing patterns, see H. E. Haber and G. L. Kane, Phys. Repts. (to appear)

18. S. Dimopoulos, Nucl. Phys. B168, 69 (1980)

19. M. E. Peskin, Nucl. Phys. B175, 197 (1980)

20. R. Barbieri, L. Maiani, and R. Petronzio, Phys. Lett. 96B, 63 (1980)

21. S. Yamada, in Proceedings of the 1983 International Symposium on Lepton and Photon Interactions at High Energies, D. G. Cassel and D. L. Kreinick, eds. (Cornell University, Ithaca, 1983)

22. M. Abolins, *et. al.*, in ref. 3

23. L. M. Jones and H. W. Wyld, Phys. Rev. D17, 759 (1978); H. Fritzsch and K.-H. Streng, Phys. Lett. 72B, 385 (1978); J. Babcock, D. Sivers, and S. Wolfram, Phys. Rev. D18, 162 (1978)

24. K. D. Lane, in ref. 3

25. J. Ellis, M. K. Gaillard, D. Nanopoulos, and P. Sikivie, Nucl. Phys. B182, 529 (1981)

26. J. Ellis, M. K. Gaillard, and D. Nanopoulos, Nucl. Phys. B106, 292 (1976)

27. J. Leveille, Phys. Lett. 83B, 123 (1979). The result can also be extracted from the work of R. N. Cahn, M. S. Chanowitz, and N. Fleishon, Phys. Lett. 82B, 113 (1979); we thank R. Cahn for performing this check.

28. L. Resnick, M. K. Sundaresan, and and P. S. Watson, Phys. Rev. D8, 172 (1973)

FIGURE CAPTIONS

1. Ellipses locating the products of electron-quark elastic scattering, for 20 TeV protons colliding with electrons of 5, 15, 70, and 250 GeV, from ref. 7. The two curves in each plot correspond to $x = 0.5$ and $x = 1$.

2. Processes present in the standard gauge theory of strong, weak, and electromagnetic interactions which dominate the *e-p* cross-section at high energies: (a) *e-q* neutral-current scattering; (b) *e-q* charged-current scattering; and (c) quark pair production by photon-gluon fusion.

3. Neutral current *e-p* cross-section at high energy, integrated over values of Q^2 greater than $f \cdot s$, for $f = 0.001, 0.01, 0.05, 0.1, 0.2$. The results incorporate the restriction that the parton lab angle be greater than 2° (solid curves) or 10° (dashed curves).

4. Charged-current cross-section in high-energy *e-p* reactions. The notation is the same as in Figure 3.

5. Cross section for quark pair production in high energy *e-p* collisions *via* the photon-gluon fusion process. The three sets of curves represent the cross-sections for producing quark jets with transverse momentum greater than 25 GeV, 50 GeV, and 100 GeV, respectively. The solid and dashed curves include angle cuts at 2° and 10°, respectively, as in Fig. 3.

6. Total cross-section for reactions mediated by new W exchange. The three sets of curves refer to various energies assumed for the electron beam colliding with a 20 TeV proton beam. Solid and dashed curves refer, as before, to angle cuts at 2° and 10°, respectively. The electron beam is assumed to be unpolarized.

7. Diagrams contributing to production of supersymmetric partners of quarks and leptons: (a) diagrams for $e+q \rightarrow \tilde{e}+\tilde{q}$; (b) diagrams for $e+q \rightarrow \tilde{\nu}+\tilde{q}$. The exchanged particles are the fermionic partners of γ, Z, and W.

8. Cross-section for $ep \rightarrow \tilde{e}+\tilde{q}$, assuming that the produced superpartners have equal masses. The three sets of curves refer, as in Fig. 6, to three different energies assumed for the electron beam. The solid and dashed curves refer to different angle cuts, as before.

9. Cross-section for $ep \rightarrow \tilde{e}+\tilde{q}$, assuming that the mass of the $\tilde{q}$ is much larger than the mass of the $\tilde{e}$. The notation is as in Fig. 8.

10. Cross-section for $ep \rightarrow \tilde{\nu}+\tilde{q}$. The notation is as in Fig. 6.

11. Cross-section for the production of the leptoquark boson predicted by technicolor models in high-energy *e-p* reactions. The three curves refer to three values of the electron beam energy.

12. Vertex leading to the photoexcitation of a light fermion f.

13. Cross-section for q^* production in high-energy *e-p* reactions. The three curves refer to three different values of the electron beam energy, as in Fig. 6. All three curves are computed setting $\Lambda = 2$ TeV.

14. Cross-section for e^* production in high-energy *e-p* reactions. The notation is as in Fig. 13.

15. Feynman diagrams contributing to supersymmetric particle production in *e-p* collisions *via* (a) $\gamma+q \rightarrow \tilde{q}+\tilde{g}$; (b) $\gamma+e \rightarrow \tilde{e}+\tilde{\gamma}$

16. Cross-section for the associated production of $\tilde{q}$ and $\tilde{g}$ in high-energy *e-p* reactions, assuming $m_{\tilde{g}} \ll m_{\tilde{q}}$.

17. Cross-section for the associated production of $\tilde{e}$ and $\tilde{\gamma}$ in high-energy *e-p* reactions. The notation is as in Fig. 6.

18. Cross-section for production of a color octet lepton $\mathcal{L}_8$ in high-energy *e-p* collisions. The notation is as in Fig. 13, and, as in that figure, we have set $\Lambda = 2$ TeV.

19. Diagrams contributing to pair-production *via* the photon-gluon fusion process.

20. Cross-section for the production of a heavy quark of charge $+\frac{2}{3}$ in high-energy *e-p* reactions. The notation is as in Fig. 6.

21. Cross-sections for the production of the heavy boson superpartners of a charge $+\frac{2}{3}$ quark. Partners of both helicities are counted. The notation is as in Fig. 6.

22. Cross-section for the production of technipion pairs in the technicolor model of ref. 18. The solid and dashed curves represent 2° and 10°angular cuts, as before.

23. Cross-section for the single production of a color-octet technipion in high-energy *e-p* collisions. The notation is as in Fig. 11. The arrow denotes the value of the mass given in ref. 19.

24. Cross-section for the production of standard Higgs boson in high-energy *e-p* collisions. The notation is as in Fig. 11.

25. Effect on $F_2(x, Q^2)$ of the contact interactions given by eq. (6.1), computed for the case of 15 GeV electrons on 20 TeV protons and $\Lambda = 2$ TeV. The curves marked LL and LR include, respectively, the effects of the first and second terms of (6.1). The dot-dash line represents the prediction of the

standard model.

26. Effect on $F_2(x, Q^2)$ of contact interactions, computed for 30 GeV electrons on 40 TeV protons and $\Lambda = 4$ TeV. The notation is as in Fig. 25.

27. Effect on $F_2(x, Q^2)$ of contact interactions, computed for 200 GeV electrons on 40 TeV protons and $\Lambda = 8$ TeV. The notation is as in Fig. 25.

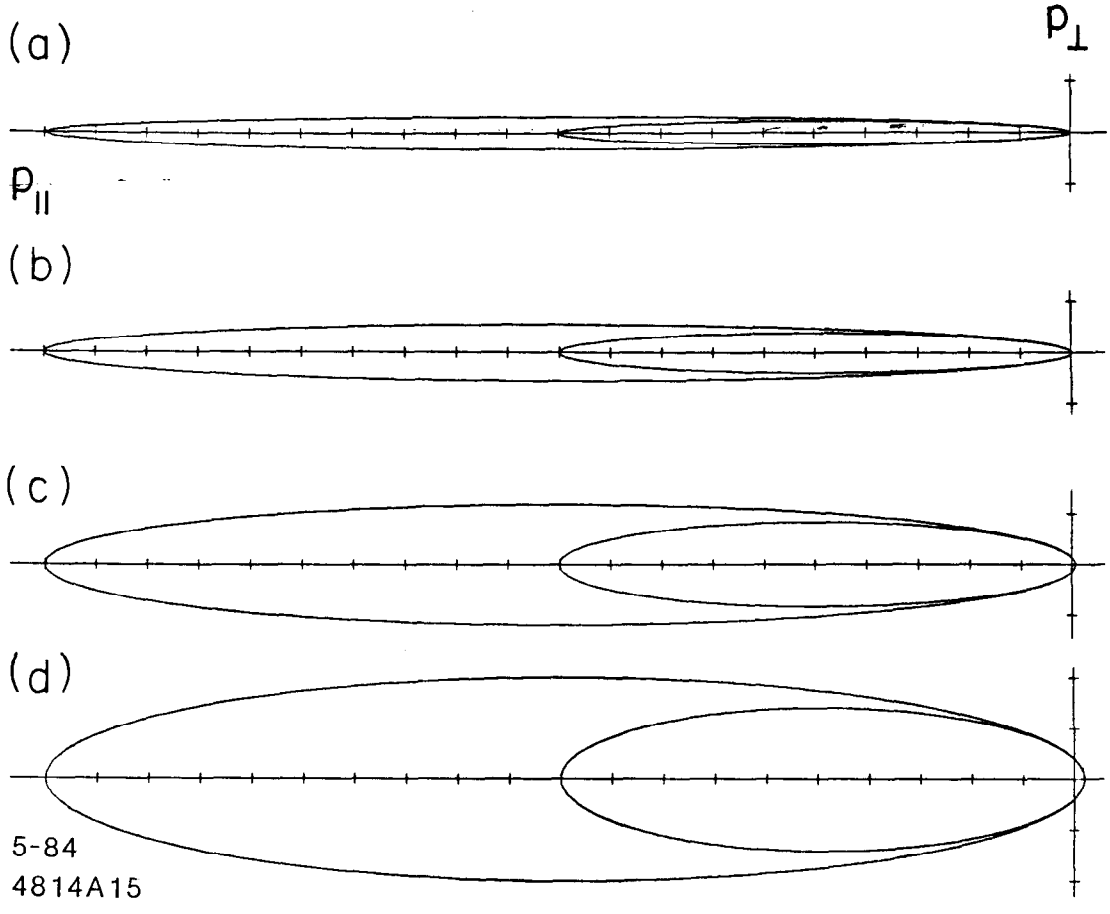

Fig. 1

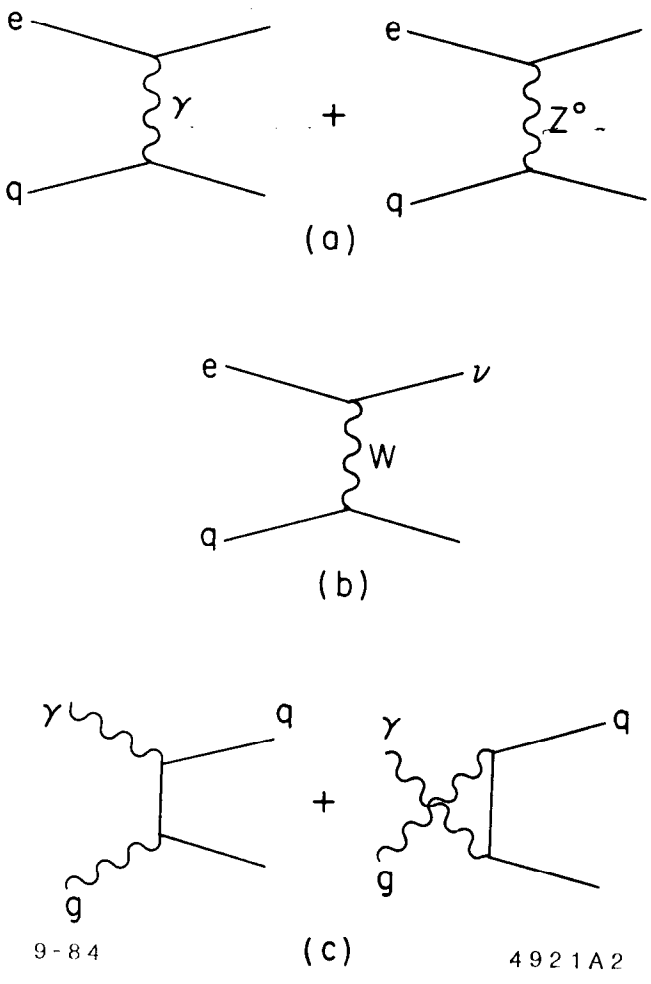

Fig. 2

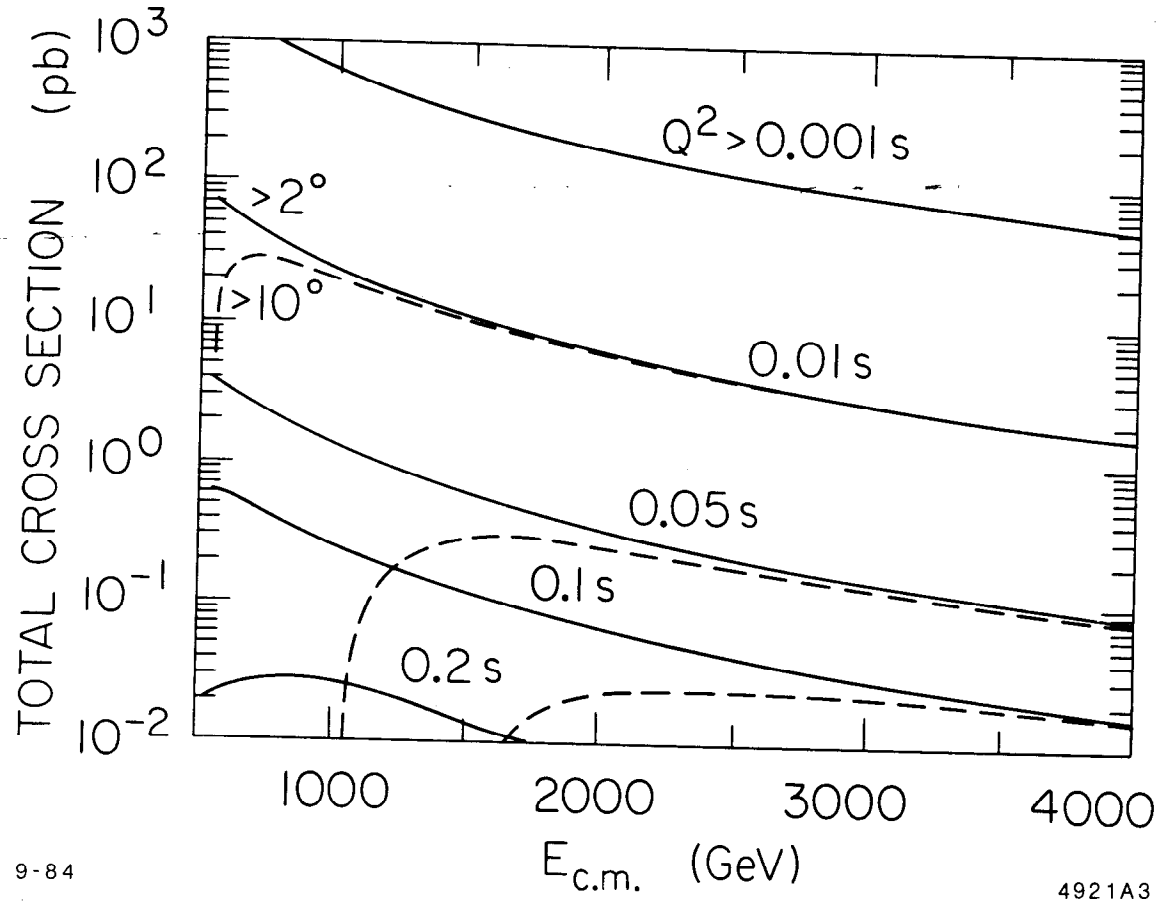
TOTAL CROSS SECTION (pb)
10^3
10^2
10^1
10^0
10^{-1}
10^{-2}
$Q^2 > 0.001\,s$
>2°
>10°
0.01 s
0.05 s
0.1 s
0.2 s
1000
2000
3000
4000
$E_{c.m.}$ (GeV)
9-84
4921A3

Fig. 3

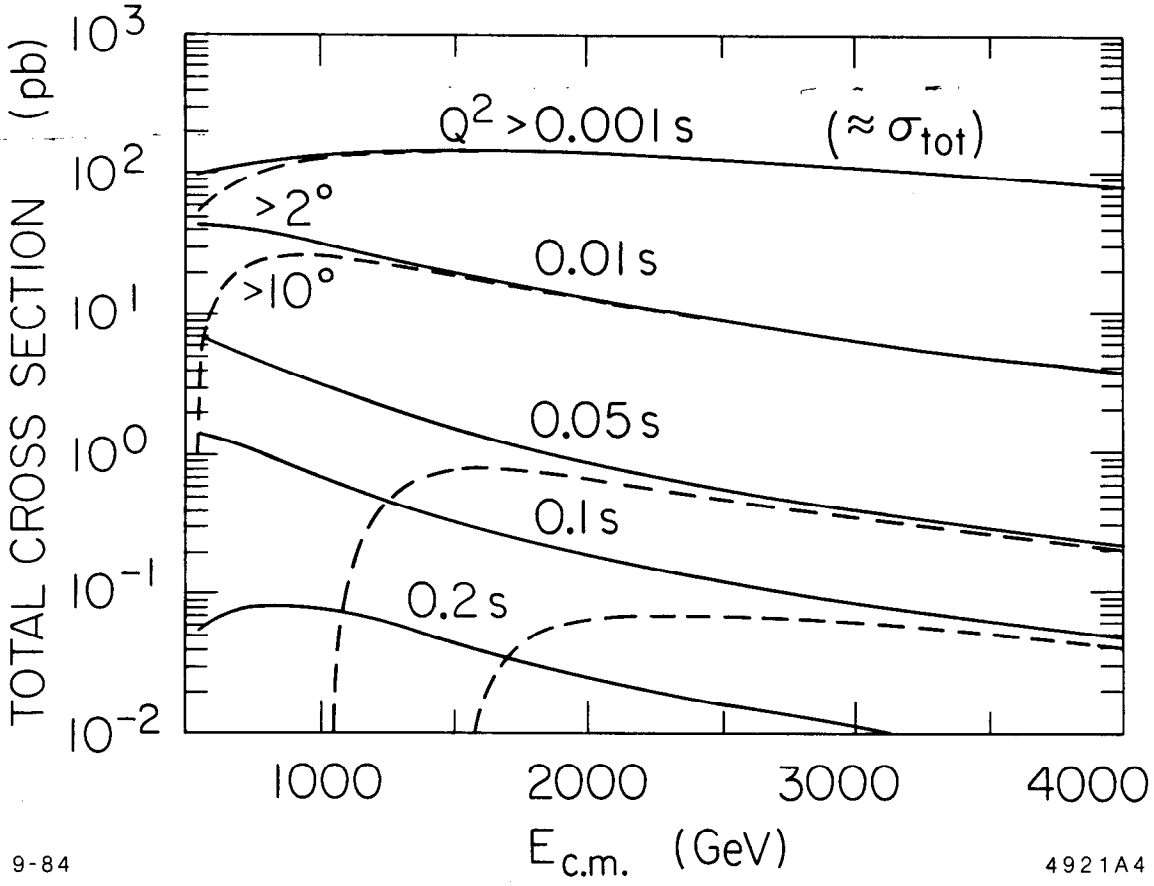
TOTAL CROSS SECTION (pb)
10^3
10^2
10^1
10^0
10^{-1}
10^{-2}
$Q^2 > 0.001\,s$ ($\approx \sigma_{tot}$)
>2°
>10°
0.01 s
0.05 s
0.1 s
0.2 s
1000
2000
3000
4000
$E_{c.m.}$ (GeV)
9-84
4921A4

Fig. 4

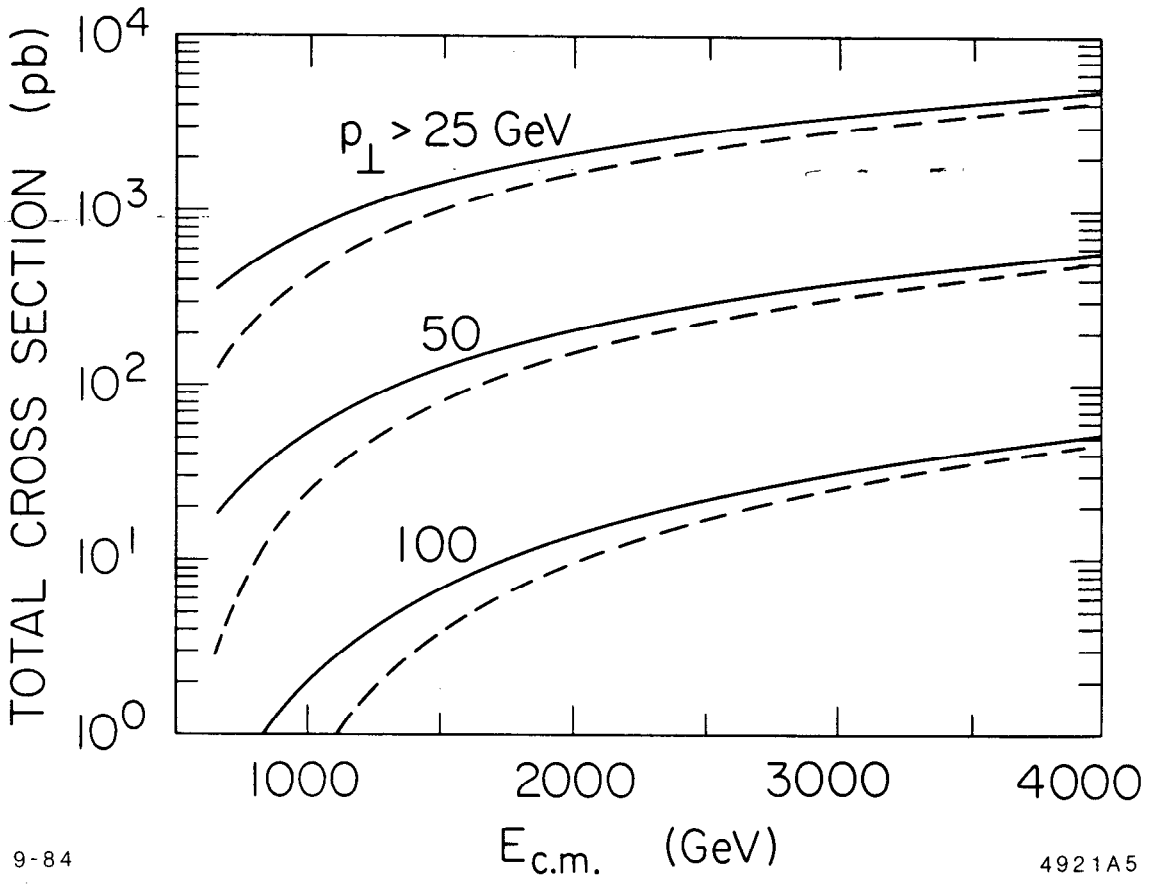
TOTAL CROSS SECTION (pb)
10^4
10^3
10^2
10^1
10^0
$p_\perp > 25$ GeV
50
100
1000
2000
3000
4000
$E_{c.m.}$ (GeV)
9-84
4921A5

Fig. 5

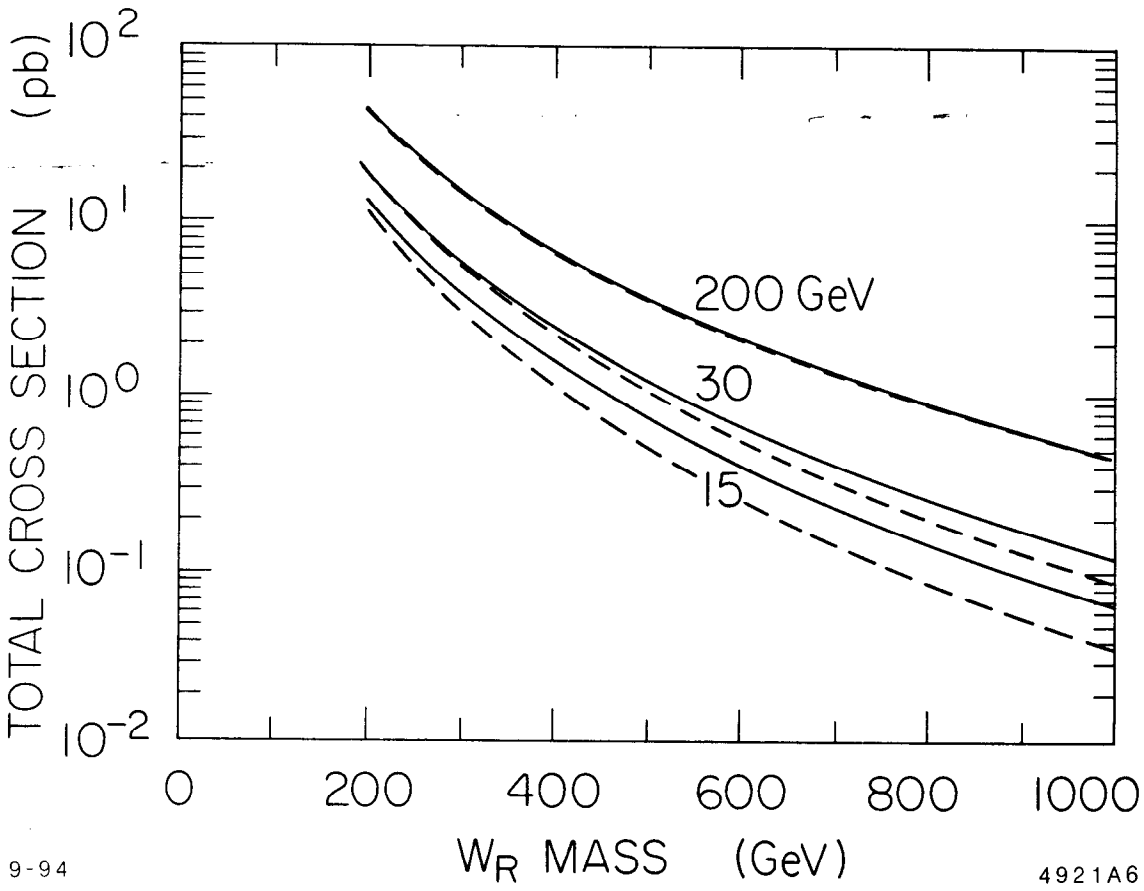
TOTAL CROSS SECTION (pb)
10^2
10^1
10^0
10^{-1}
10^{-2}
200 GeV
30
15
0
200
400
600
800
1000
W_R MASS (GeV)
9-94
4921A6

Fig. 6

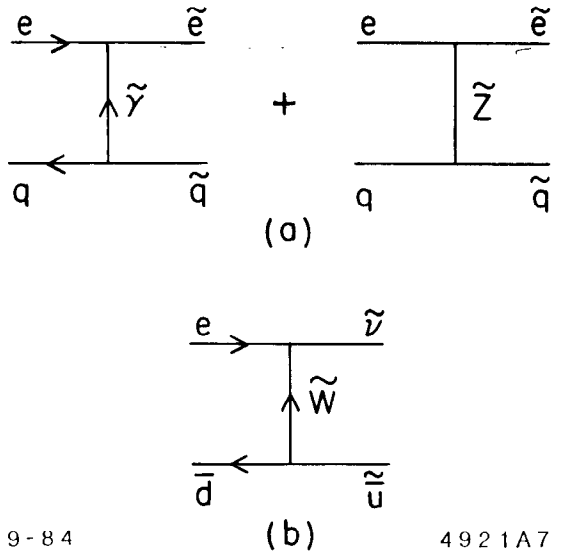

Fig. 7

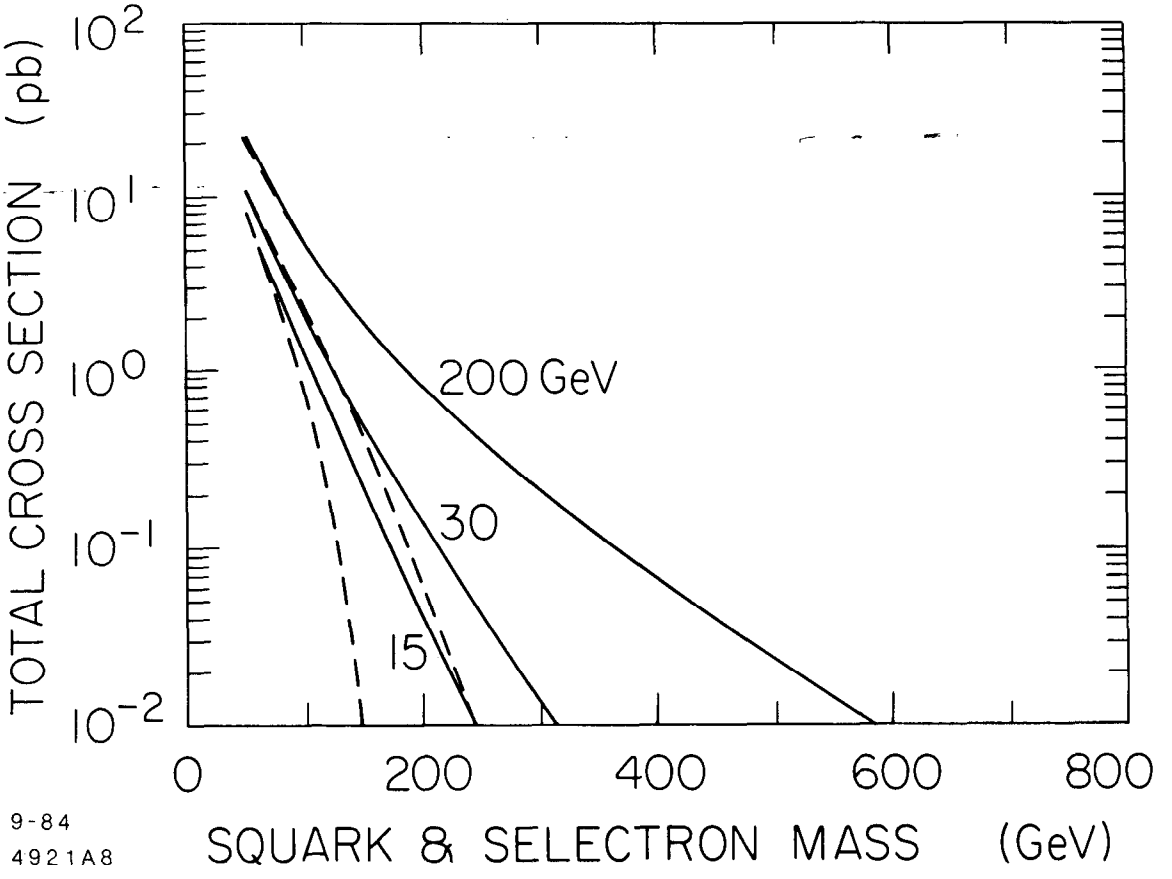
TOTAL CROSS SECTION (pb)
10^2
10^1
10^0
10^{-1}
10^{-2}
200 GeV
30
15
0
200
400
600
800
SQUARK & SELECTRON MASS (GeV)
9-84
4921A8

Fig. 8

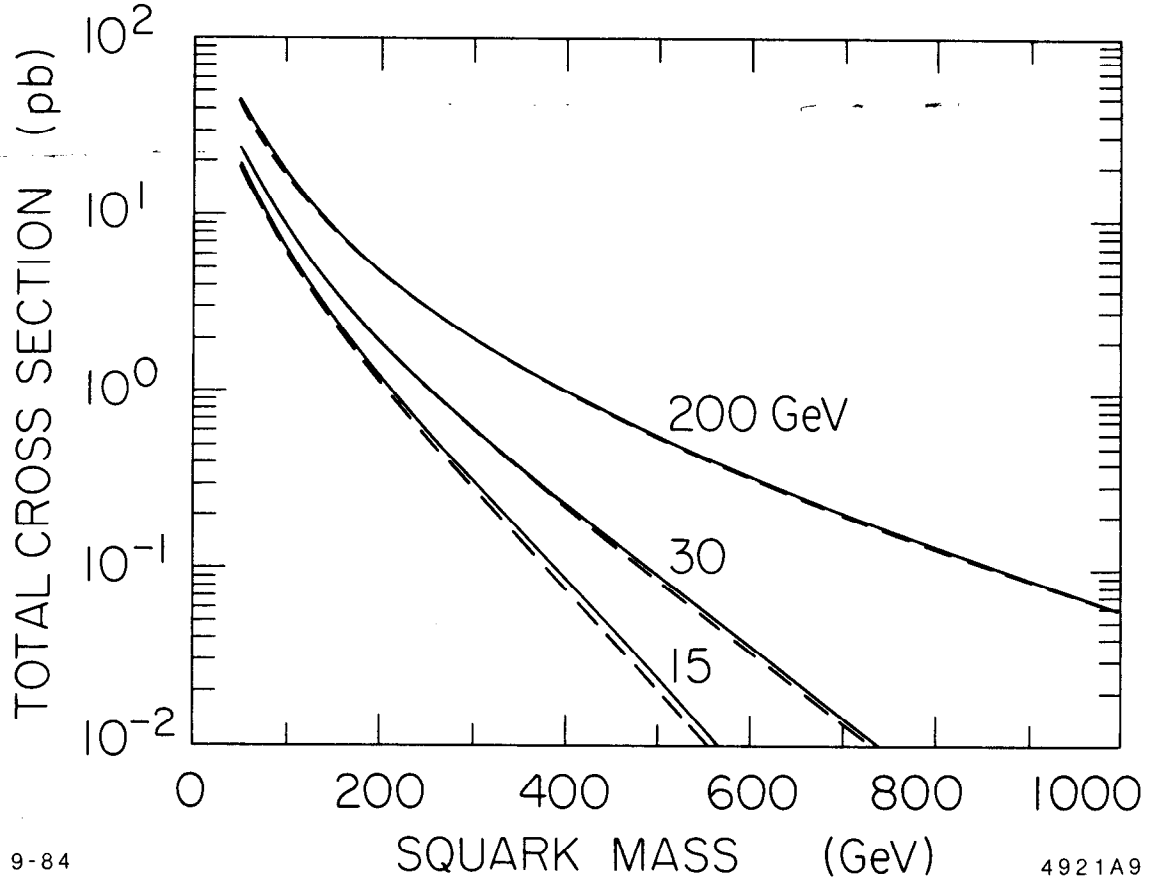
TOTAL CROSS SECTION (pb)
10^2
10^1
10^0
10^{-1}
10^{-2}
200 GeV
30
15
0
200
400
600
800
1000
SQUARK MASS (GeV)
9-84
4921A9

Fig. 9

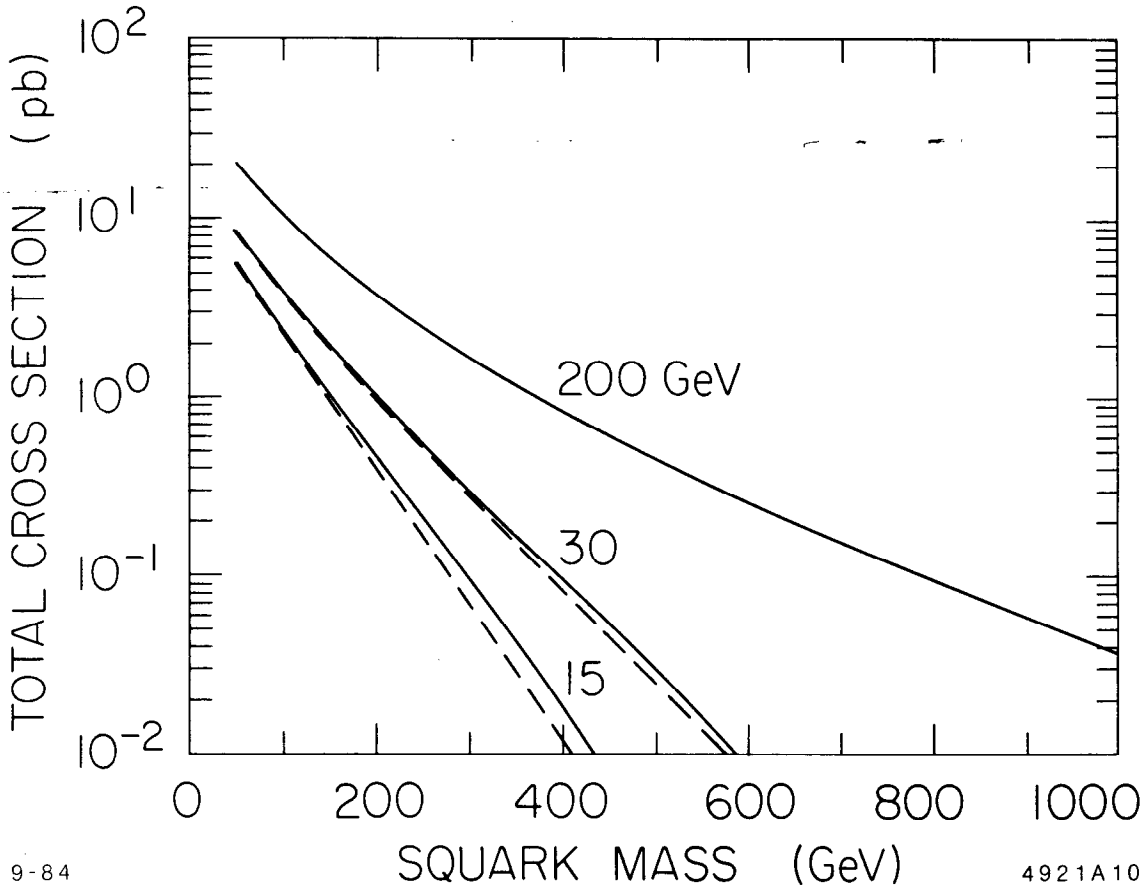
TOTAL CROSS SECTION (pb)
10^2
10^1
10^0
10^{-1}
10^{-2}
200 GeV
30
15
0
200
400
600
800
1000
SQUARK MASS (GeV)
9-84
4921A10

Fig. 10

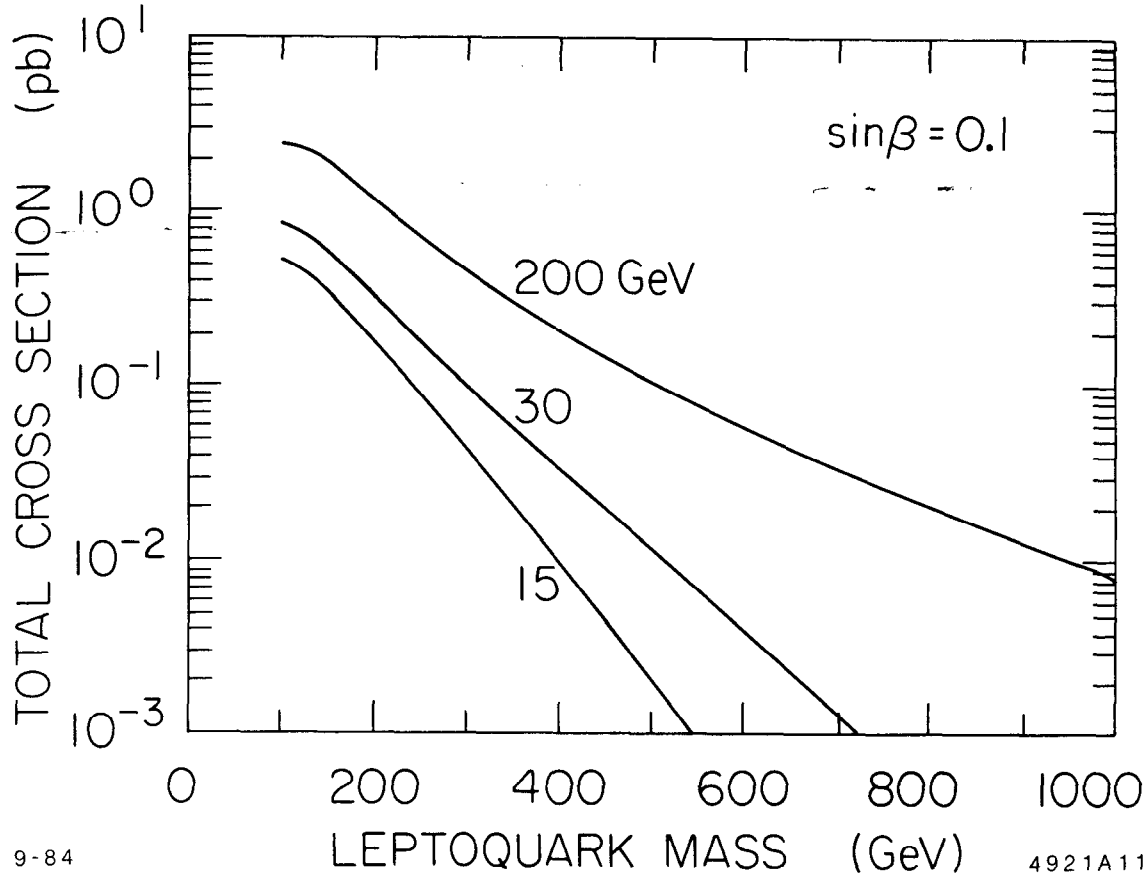
TOTAL CROSS SECTION (pb)
10^{1}
10^{0}
10^{-1}
10^{-2}
10^{-3}
$\sin\beta = 0.1$
200 GeV
30
15
0
200
400
600
800
1000
LEPTOQUARK MASS (GeV)
9-84
4921A11

Fig. 11

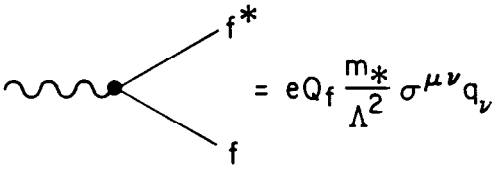

9-84 4921A12

Fig. 12

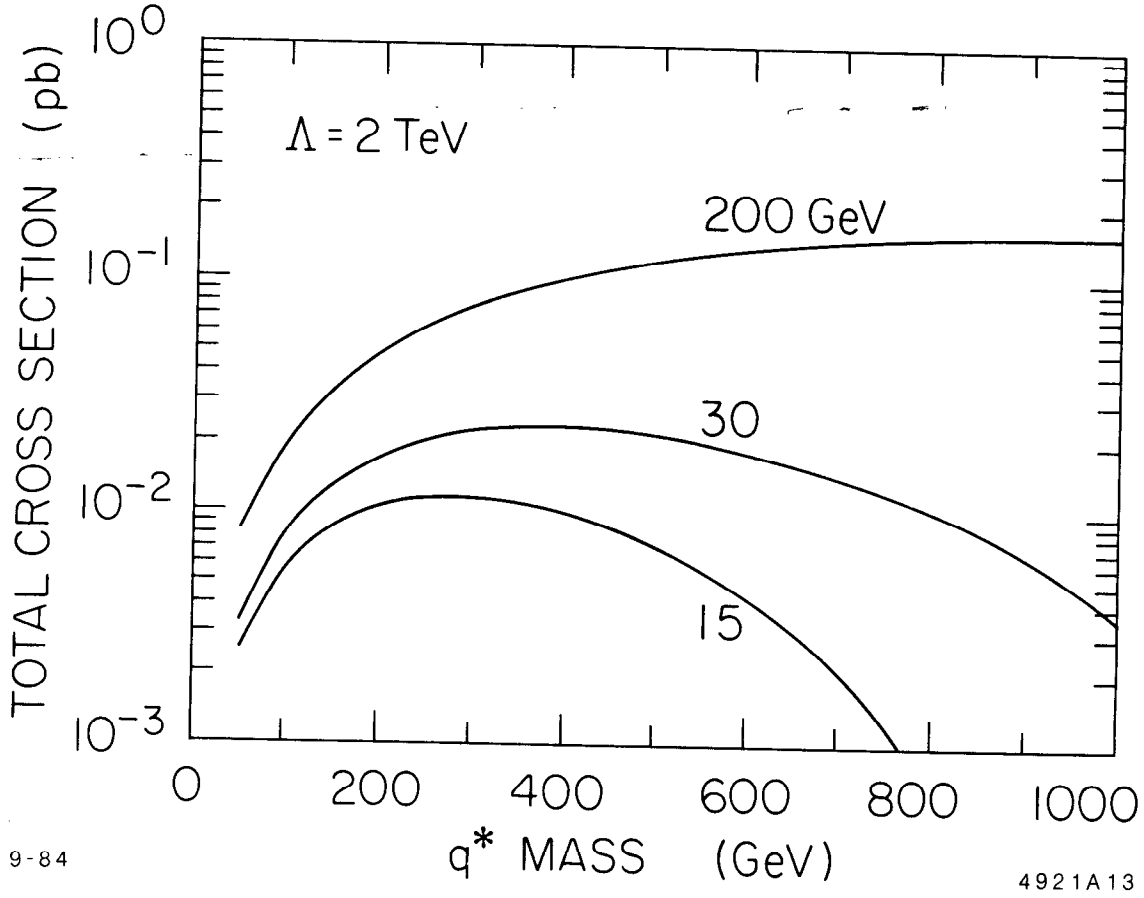
TOTAL CROSS SECTION (pb)
10^0
10^{-1}
10^{-2}
10^{-3}
Λ = 2 TeV
200 GeV
30
15
0
200
400
600
800
1000
q* MASS (GeV)
9-84
4921A13

Fig. 13

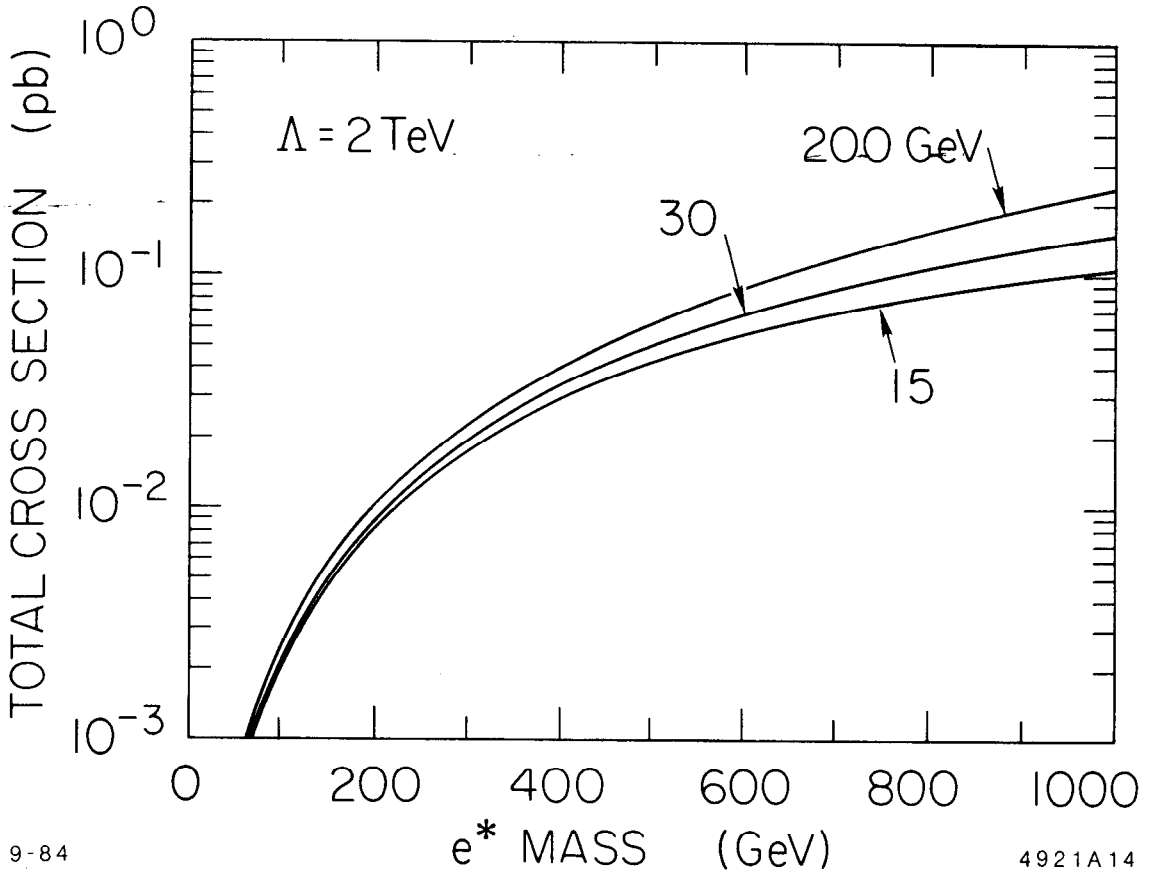
TOTAL CROSS SECTION (pb)
10^0
10^{-1}
10^{-2}
10^{-3}
Λ = 2 TeV
200 GeV
30
15
0
200
400
600
800
1000
e* MASS (GeV)
9-84
4921A14

Fig. 14

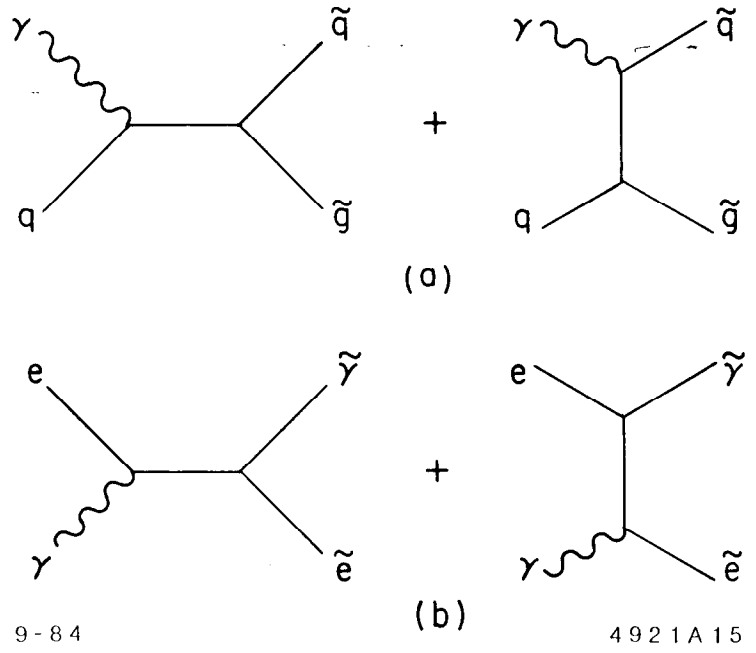

Fig. 15

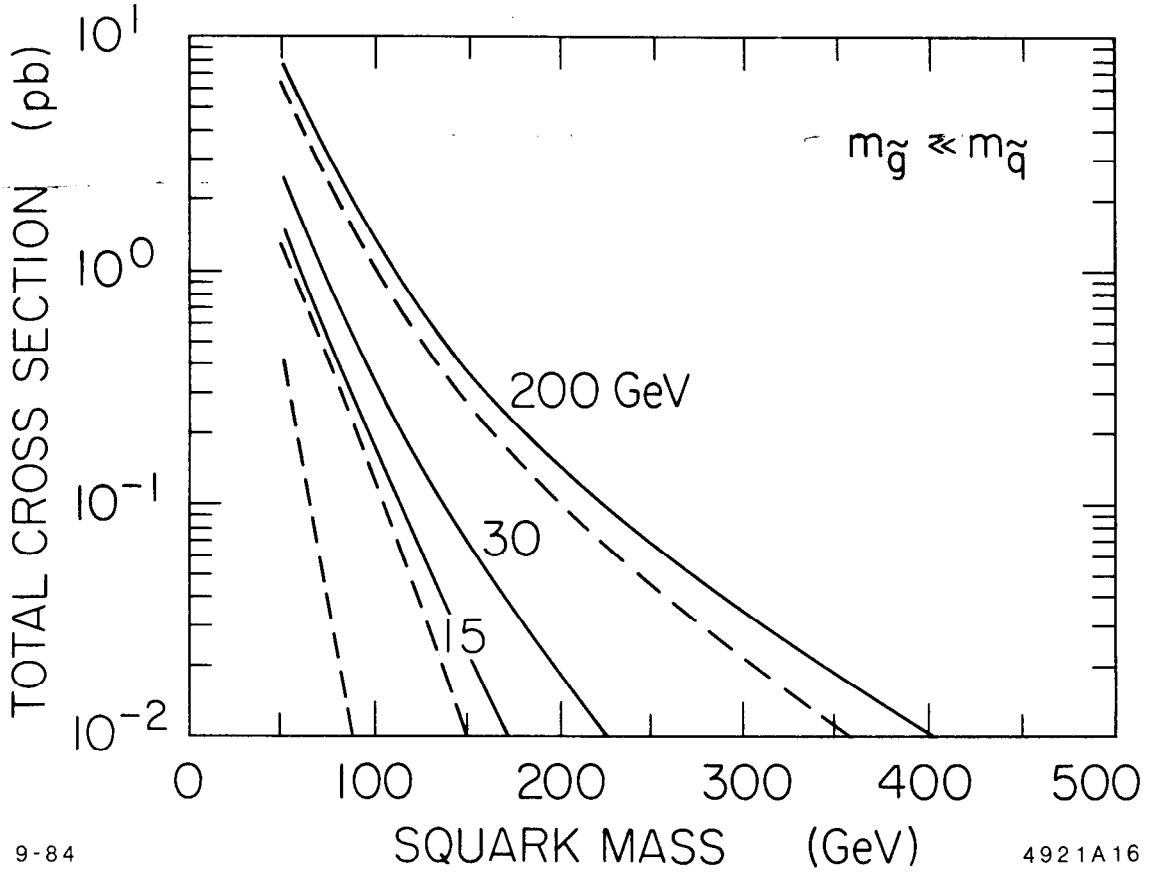
TOTAL CROSS SECTION (pb)
10^1
10^0
10^{-1}
10^{-2}
$m_{\tilde{g}} \ll m_{\tilde{q}}$
200 GeV
30
15
0
100
200
300
400
500
SQUARK MASS (GeV)
9-84
4921A16

Fig. 16

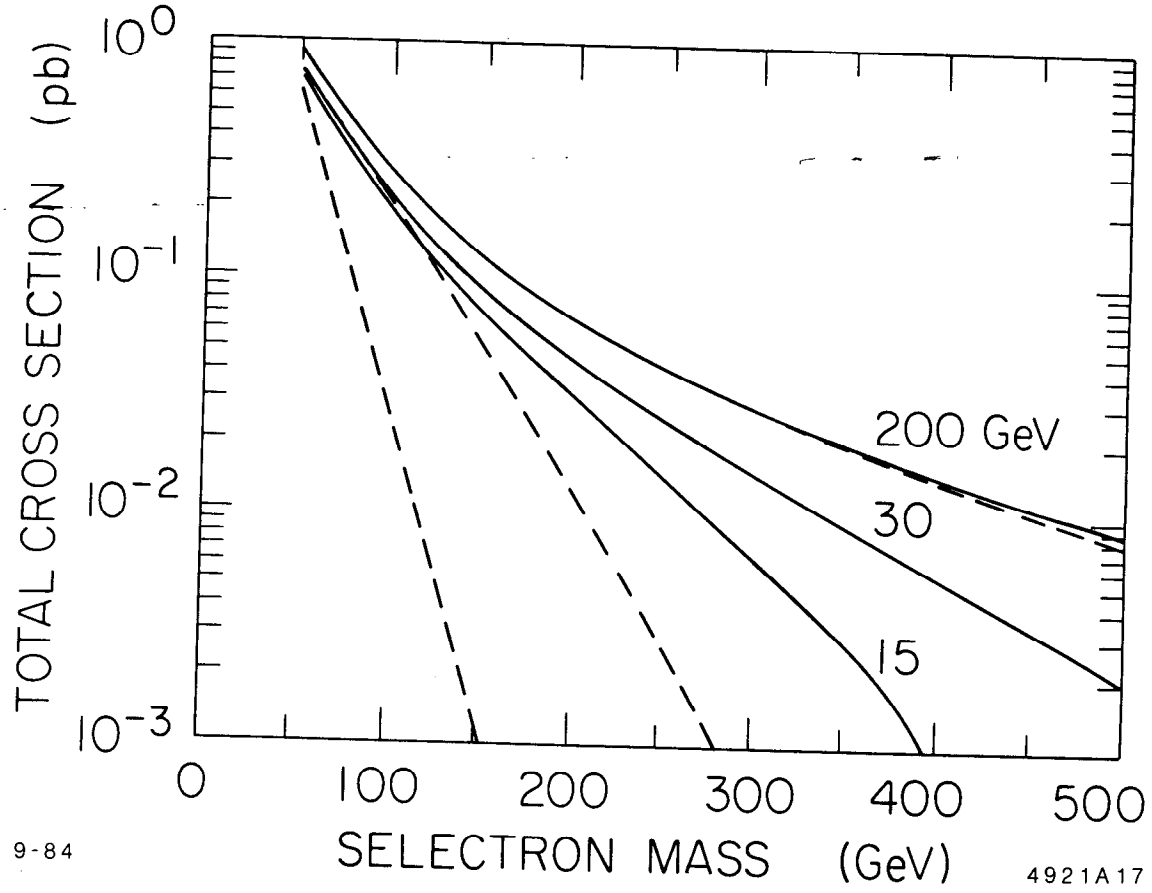
TOTAL CROSS SECTION (pb)
10^0
10^{-1}
10^{-2}
10^{-3}
0
100
200
300
400
500
SELECTRON MASS (GeV)
200 GeV
30
15
9-84
4921A17

Fig. 17

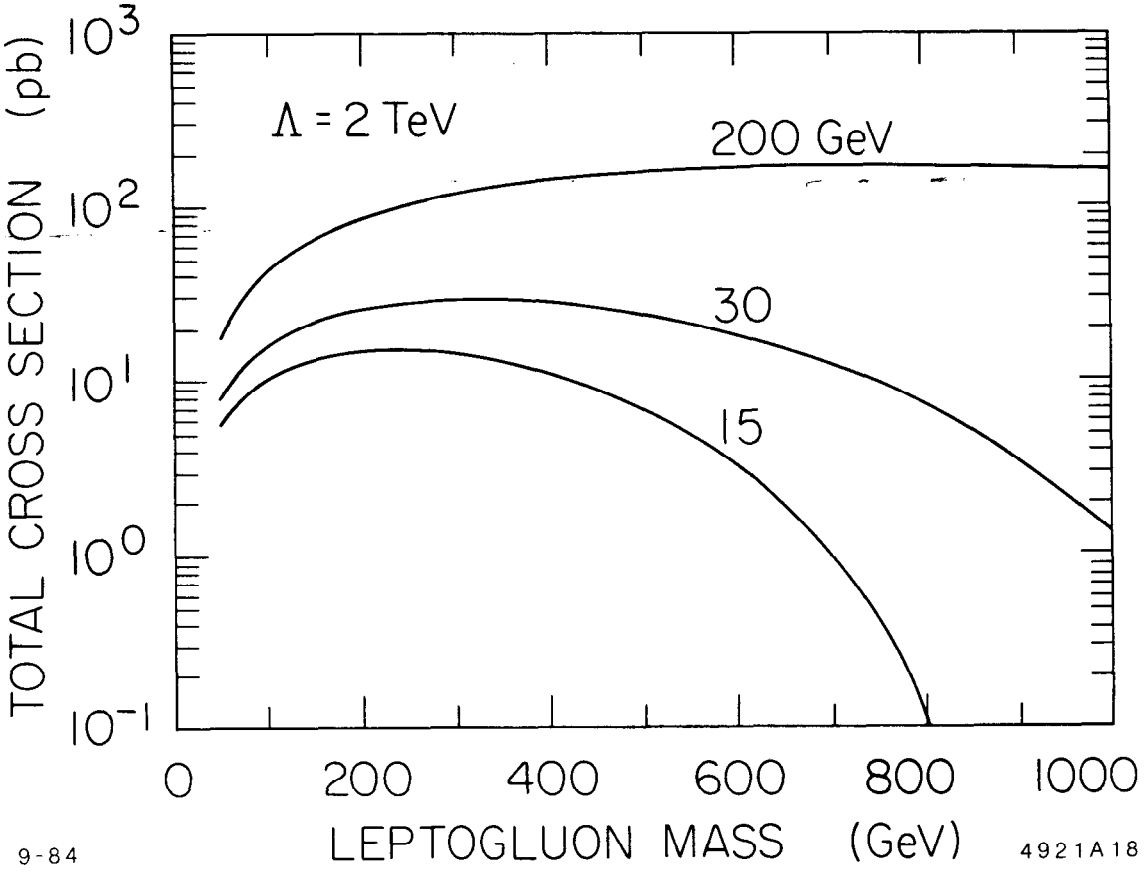
TOTAL CROSS SECTION (pb)
10^3
10^2
10^1
10^0
10^{-1}
Λ = 2 TeV
200 GeV
30
15
0
200
400
600
800
1000
LEPTOGLUON MASS (GeV)
9-84
4921A18

Fig. 18

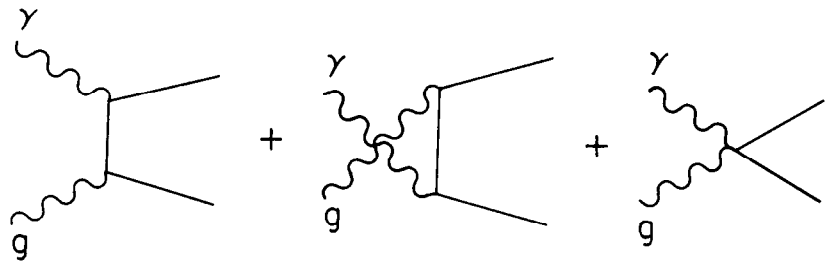

9-84

4921A19

Fig. 19

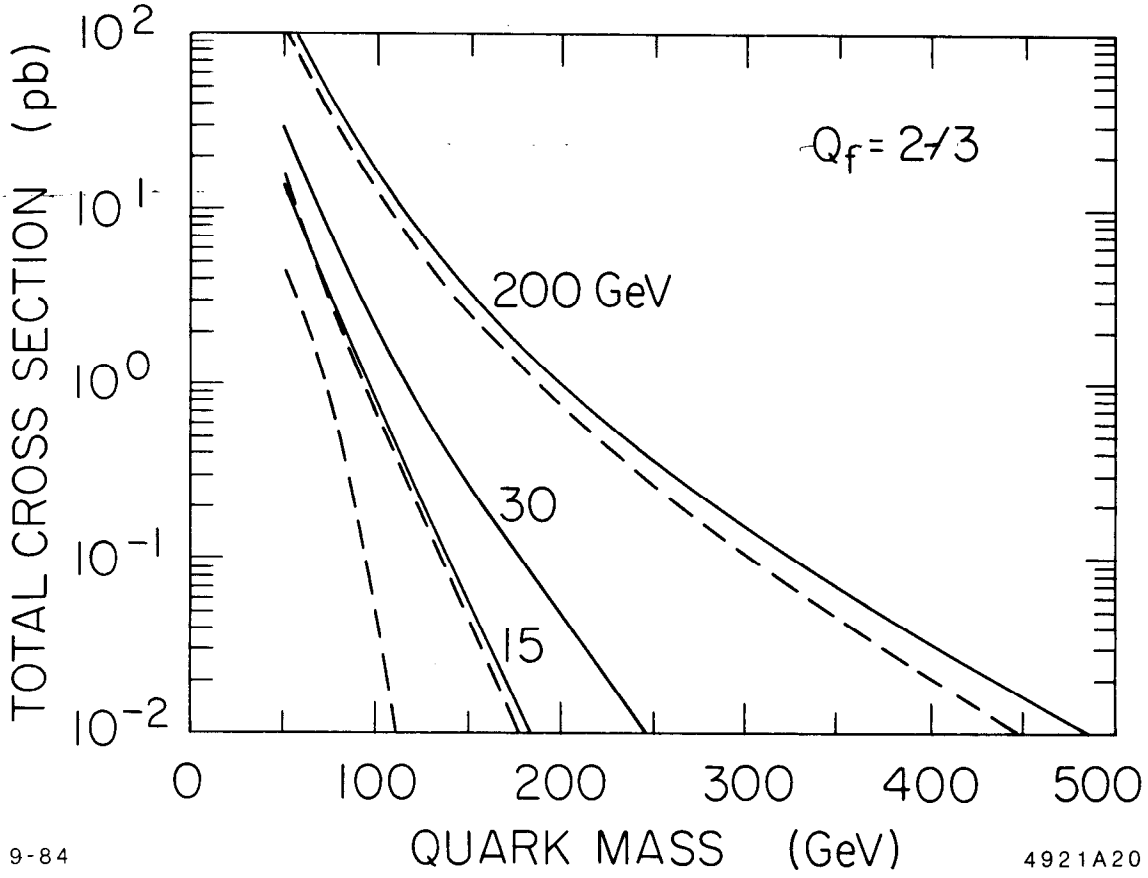
TOTAL CROSS SECTION (pb)
10^2
10^1
10^0
10^{-1}
10^{-2}
$Q_f = 2/3$
200 GeV
30
15
0
100
200
300
400
500
QUARK MASS (GeV)
9-84
4921A20

Fig. 20

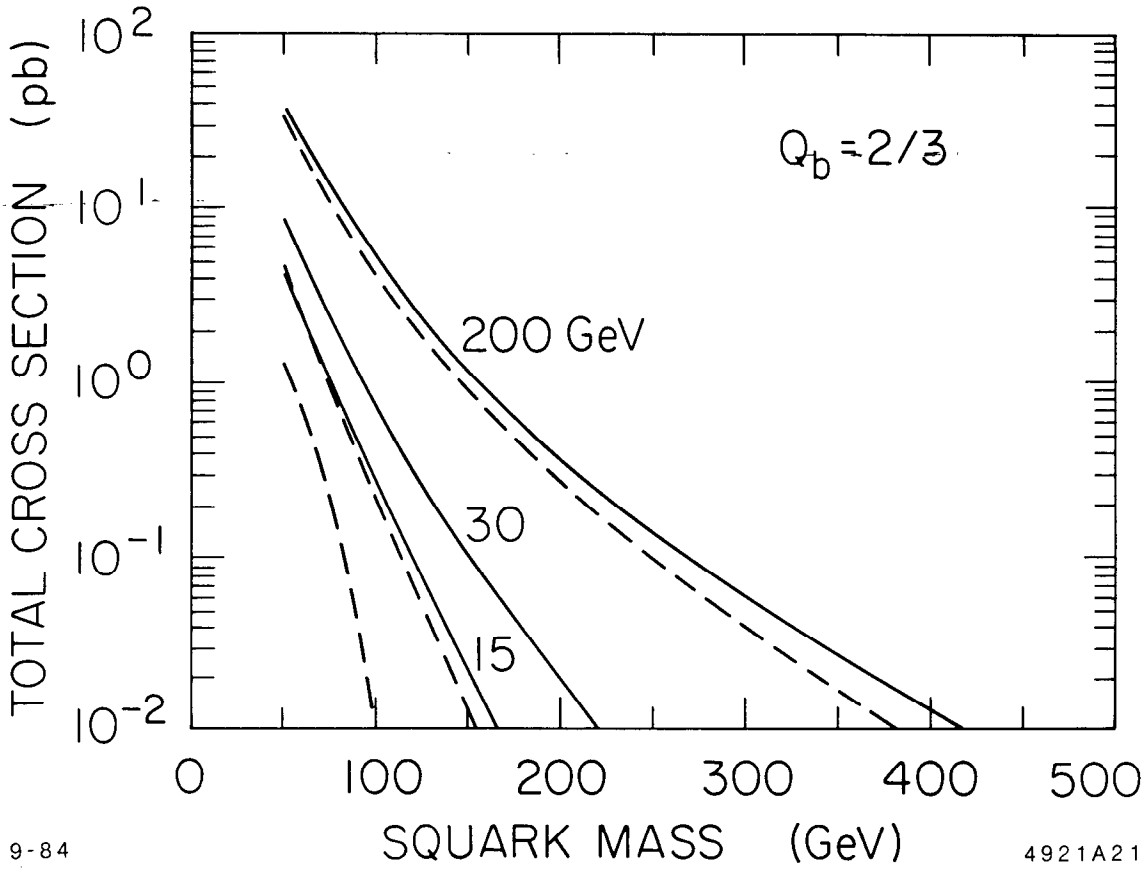
TOTAL CROSS SECTION (pb)
10^2
10^1
10^0
10^{-1}
10^{-2}
$Q_b = 2/3$
200 GeV
30
15
0
100
200
300
400
500
SQUARK MASS (GeV)
9-84
4921A21

Fig. 21

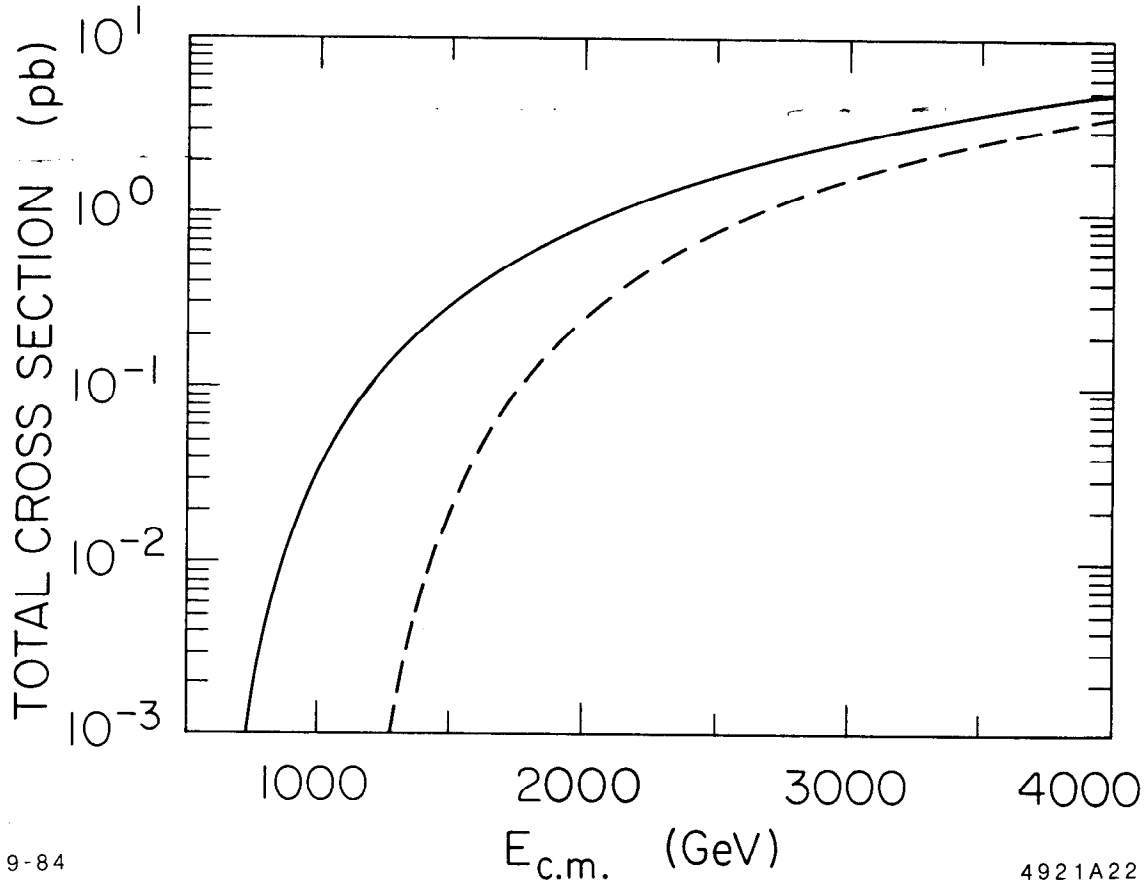
TOTAL CROSS SECTION (pb)
10^{1}
10^{0}
10^{-1}
10^{-2}
10^{-3}
1000
2000
3000
4000
$E_{c.m.}$ (GeV)
9-84
4921A22

Fig. 22

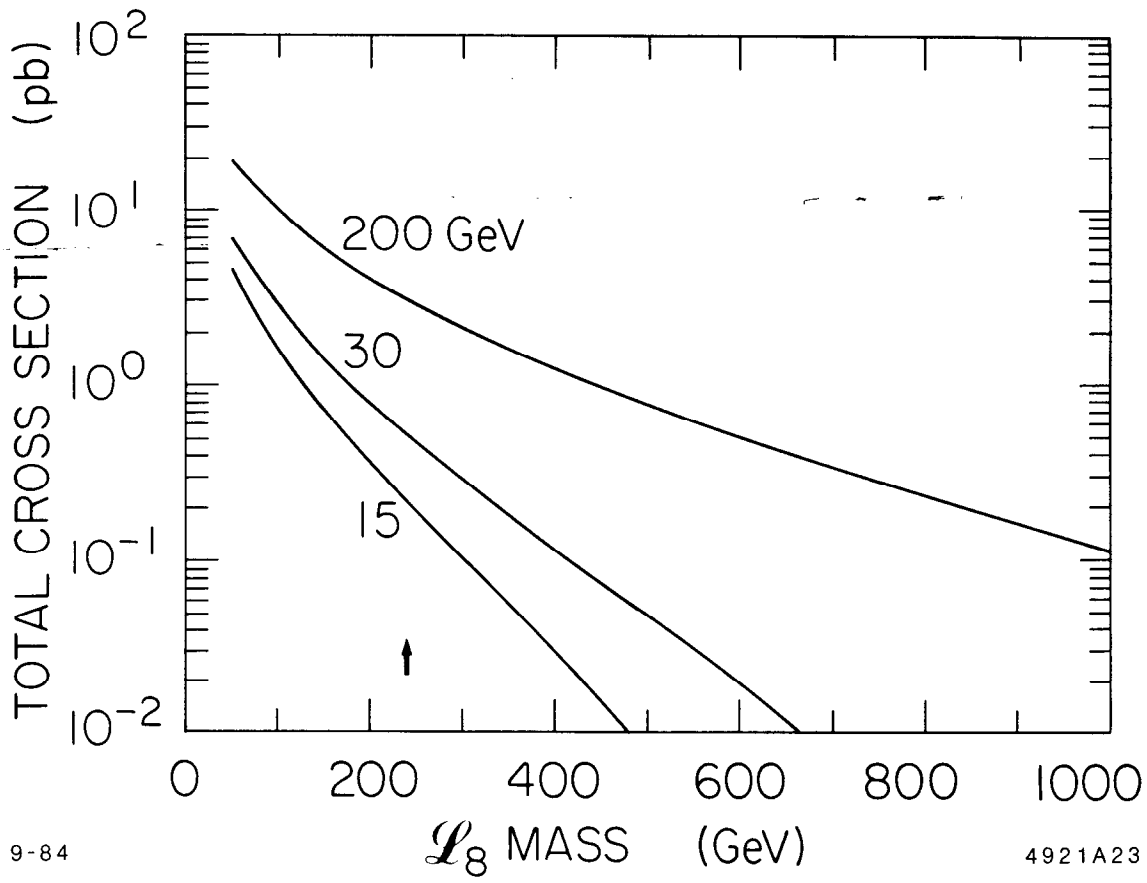
TOTAL CROSS SECTION (pb)
10^2
10^1
10^0
10^{-1}
10^{-2}
200 GeV
30
15
0
200
400
600
800
1000
$\mathscr{L}_8$ MASS (GeV)
9-84
4921A23

Fig. 23

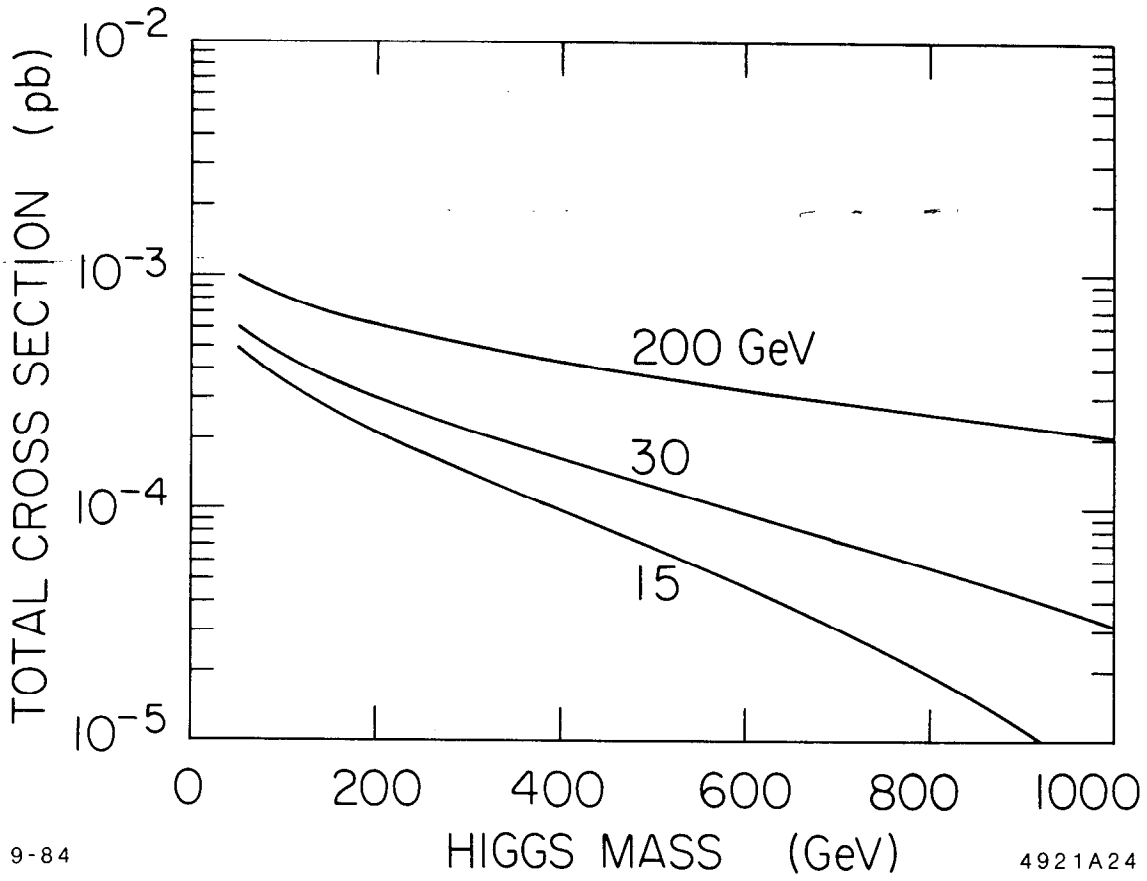
TOTAL CROSS SECTION (pb)
10^{-2}
10^{-3}
10^{-4}
10^{-5}
200 GeV
30
15
0
200
400
600
800
1000
HIGGS MASS (GeV)
9-84
4921A24

Fig. 24

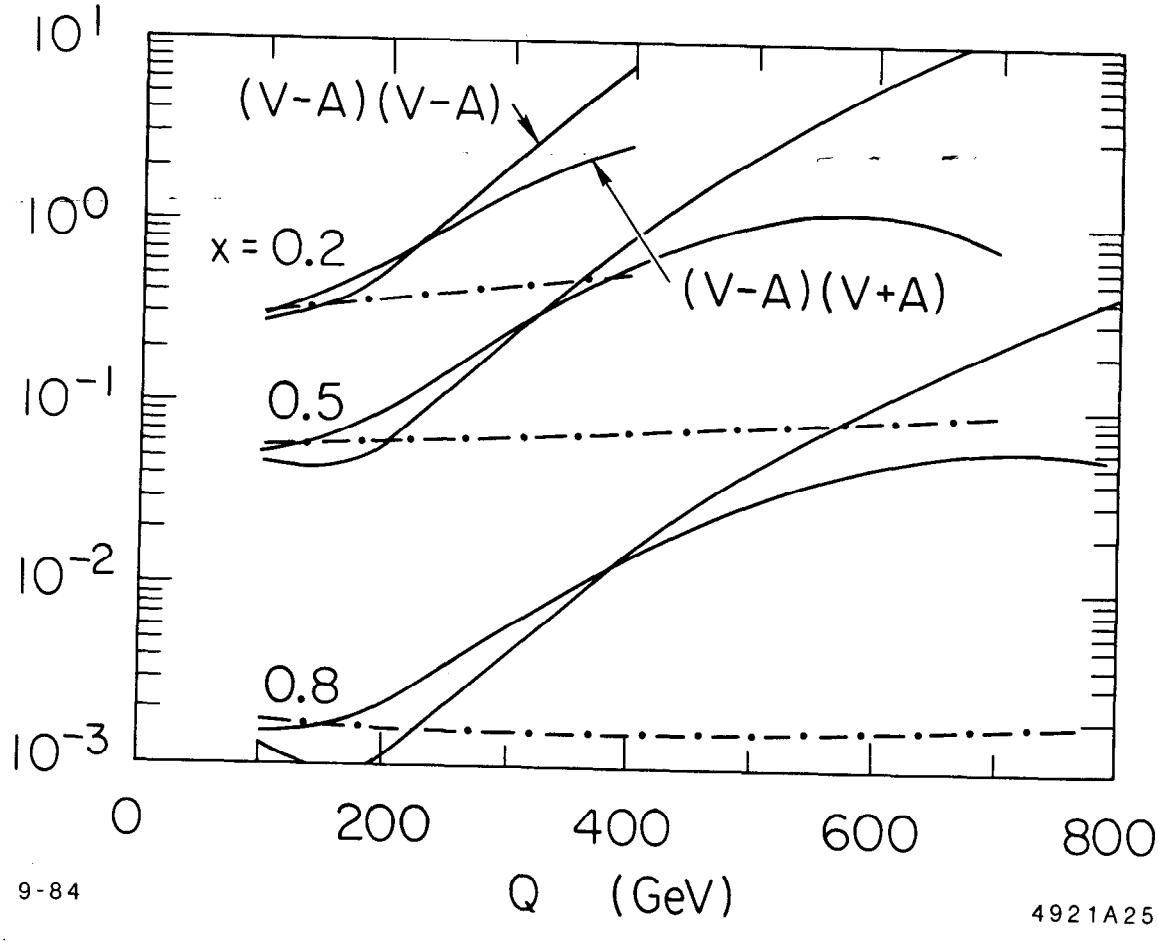
10^1
10^0
10^{-1}
10^{-2}
10^{-3}
(V-A)(V-A)
x = 0.2
(V-A)(V+A)
0.5
0.8
0
200
400
600
800
Q (GeV)
9-84
4921A25

Fig. 25

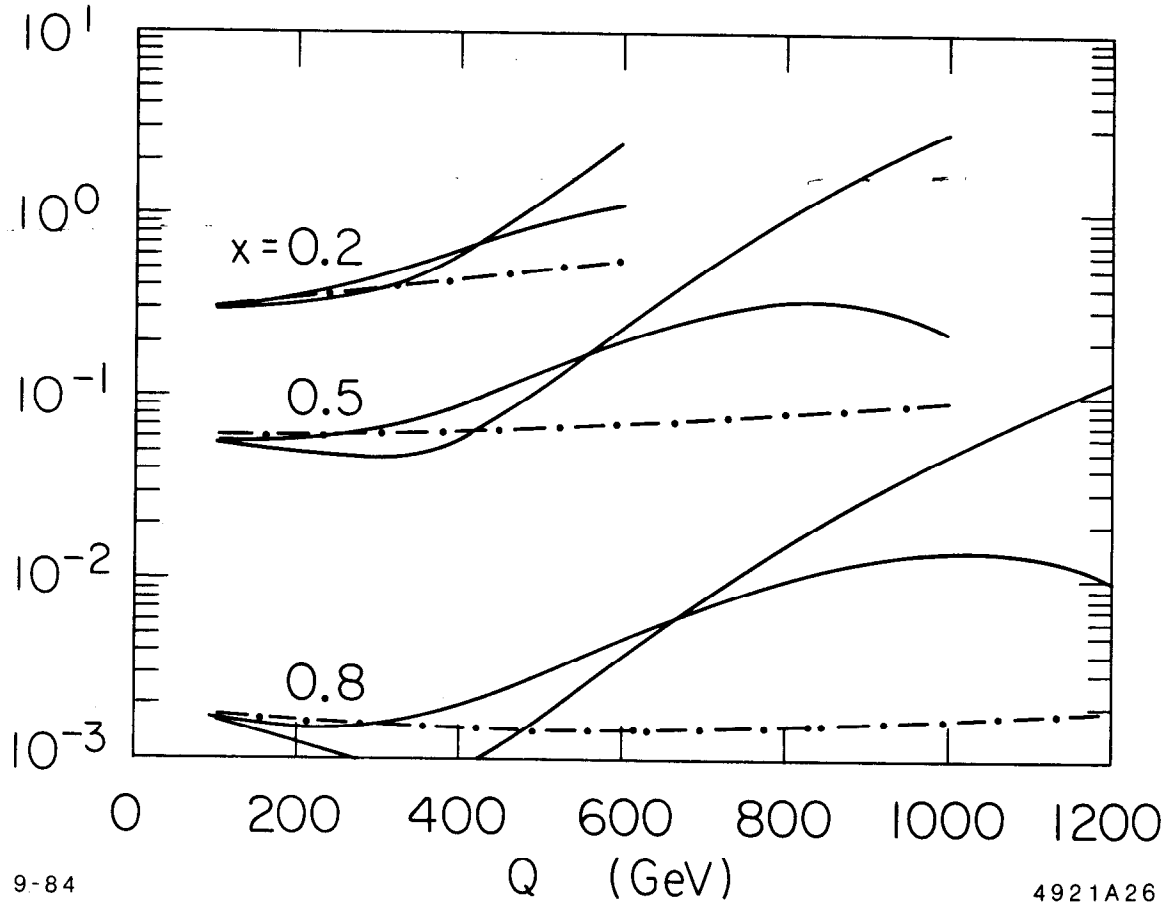
10^1
10^0
10^{-1}
10^{-2}
10^{-3}
x = 0.2
0.5
0.8
0
200
400
600
800
1000
1200
Q (GeV)
9-84
4921A26

Fig. 26

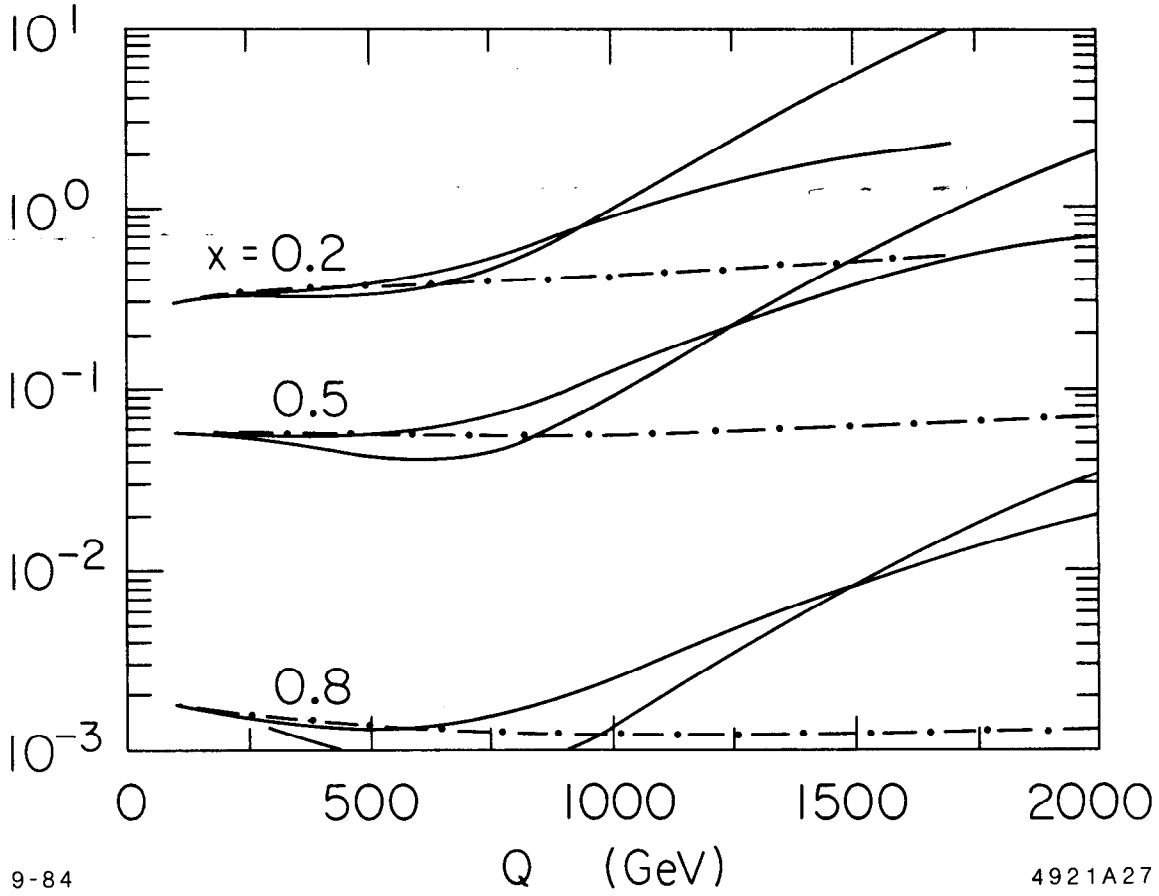
10^1
10^0
10^{-1}
10^{-2}
10^{-3}
x = 0.2
0.5
0.8
0
500
1000
1500
2000
Q (GeV)
9-84
4921A27

Fig. 27